

Reconstructing 20th century global hydrography: a contribution to the Global Terrestrial Network- Hydrology (GTN-H)

D. Wisser¹, B. M. Fekete², C. J. Vörösmarty², and A. H. Schumann³

¹Institute for the Study of Earth, Oceans, and Space, University of New Hampshire, Durham, New Hampshire, USA

²Civil Engineering Department, City College of New York, CUNY, New York, USA

³Institute of Hydrology, Water Resources Management and Environmental Engineering, Ruhr-Universität Bochum, Bochum, Germany

Received: 17 March 2009 – Published in Hydrol. Earth Syst. Sci. Discuss.: 26 March 2009

Revised: 4 November 2009 – Accepted: 4 November 2009 – Published: 6 January 2010

Abstract. This paper presents a new reconstruction of the 20th century global hydrography using fully coupled water balance and transport model in a flexible modeling framework. The modeling framework allows a high level of configurability both in terms of input forcings and model structure. Spatial and temporal trends in hydrological cycle components are assessed under “pre-industrial” conditions (without modern-day human activities) and contemporary conditions (incorporating the effects of irrigation and reservoir operations). The two sets of simulations allow the isolation of the trends arising from variations in the climate input driver alone and from human interventions. The sensitivity of the results to variations in input data was tested by using three global gridded datasets of precipitation.

Our findings confirm that the expansion of irrigation and the construction of reservoirs has significantly and gradually impacted hydrological components in individual river basins. Variations in the volume of water entering the oceans annually, however, are governed primarily by variations in the climate signal alone with human activities playing a minor role. Globally, we do not find a significant trend in the terrestrial discharge over the last century.

The largest impact of human intervention on the hydrological cycle arises from the operation of reservoirs that drastically changes the seasonal pattern of horizontal water transport in the river system and thereby directly and indirectly affects a number of processes such as ability to decompose organic matter or the cycling of nutrients in the river system.

1 Introduction

Humans have greatly altered the hydrological cycle over the last century. Global water withdrawal has increased by 700% during the last century (Ghassemi and White, 2007) and is expected to further rise as the world’s population continues growing. Such alterations affect the magnitude and the timing of runoff and river flow, and have been amply documented. These impacts include the abstraction of water for irrigation and the distortions of discharge imposed by reservoirs altering the temporal pattern of river discharge (Bouwer et al., 2006; Haddeland et al., 2006b; Shibuo et al., 2007), and the impacts of increased evapotranspiration due to land cover changes that could potentially affect local climate. Furthermore, changes in observed streamflow over the last century and model simulations show coherent trends (increases in Eastern Africa and high-latitude regions and decreases in Southern Africa, Southern Europe and the Middle East) in the availability of freshwater predicted in a changing climate (Milly et al., 2005).

The abstraction of water for irrigation purposes lowers the volume of water entering rivers but has also been shown to impact the seasonality of river flow by increasing winter river discharge should water returning from irrigated areas become runoff (Kendy and Bredehoeft, 2006). Such alterations in the hydrological cycle do not only impact the spatial and temporal distribution of runoff but have direct and indirect effects on the bio-geophysical state of water resources and thereby on the sustainability of water resources.

The changes in the apparent aging of water on river systems as a result of reservoir impoundments, greatly affect the re-aeration capacity of the river, which in turn, determines the ability of the water to decompose organic matter. Reservoirs impact the sediment retention of major rivers (Vörösmarty et al., 2003), the emission of trace gas



Correspondence to: D. Wisser
(dominik.wisser@unh.edu)

(Galy-Lacaux et al., 1999; Soumis et al., 2004; St. Louis et al., 2000) and the cycling of nutrients (Seitzinger et al., 2002). The global water cycle is therefore not affected by the changes in the weather and climate system alone but also by additional sources of human interventions (Vörösmarty, 2002), the most notable of which at the scale this study is concerned with are increased evapotranspiration due to expansion of irrigated areas and the distortion of streamflow by large impoundments (Vörösmarty and Sahagian, 2000).

The purpose of this paper is to analyze trends in components of the global hydrological cycle over the 20th century and to investigate the contribution of human interventions to changes in those components. We use a water balance modeling approach that explicitly accounts for such interventions when forced by time series of observed climate data.

After a brief description of the model and data we present a validation of the model and discuss the sensitivity of our simulations to variations in input data sets. The validation of the model is aimed at demonstrating the model's capability to reproduce observed discharge and the impact of irrigation water abstractions.

Time series of modeled discharge (under natural and disturbed conditions) entering the oceans and internally draining basins are discussed. We illustrate the impacts of time varying irrigated areas and reservoirs for a set of representative river basins.

2 Methods

2.1 The WBM_{plus} Model

To simulate components of the hydrological cycle, we used WBM_{plus}, an extension of a grid based water balance and transport algorithm (Federer et al., 2003; Rawlins et al., 2003; Vörösmarty et al., 1998). WBM_{plus} is a fully coupled water balance and transport model that simulates the vertical water exchange between the land surface and the atmosphere and the horizontal water transport along a prescribed river network. It is implemented in the recently developed modeling Framework for Aquatic Modeling in the Earth System (FrAMES; Wollheim et al., 2008) which was designed to enable applications of coupled hydrological/biogeochemical models at scales ranging from local (grid cell size in the range of a few hundred meters) to continental and global (grid cell size ranging from 6 min to 30 min), operating at a daily time step. Modeling frameworks have been designed to increase the inter-operability and portability of software among developers, and to increase the efficiency of software development through a set of shared software systems, standards, and utilities, and the use of such frameworks have recently received considerable attention for hydrological models as well as for more complex Earth system and climate models (Dickonson et al., 2002; Wollheim et al., 2008). Besides the structural changes compared to the

previous versions of WBM/WTM (Vörösmarty et al., 1998), the most important new elements in WBM_{plus} are modules that explicitly account for the human activities such as irrigation water abstractions (Wisser et al., 2008) and reservoir operation directly affecting the water cycle processes.

2.2 Water balance calculations

The water balance calculations representing vertical water exchange between the atmosphere and the land surface are performed for rain-fed and irrigated areas separately. Each grid cell is partitioned into irrigated and non-irrigated parts and the water budget over the whole cell is computed as the area weighted average of the two parts.

2.2.1 Snowpack

WBM_{plus} implements an improved snowpack simulation over previous versions. The snowpack is calculated uniformly over irrigated and non-irrigated areas. Precipitation is considered snow if the daily mean air temperature is below a snowfall threshold SF (set to -1°C) and rain above that threshold. The snow accumulates during the snowing period without allowing sublimation. During the melting periods when snow is on the ground and the temperature is above a snowmelt threshold (1°C), the snowmelt M_s [mm d^{-1}] is computed as function of mean daily temperature T_m [$^\circ\text{C}$] and daily precipitation P [mm d^{-1}] (Willmott et al., 1985):

$$M_s = 2.63 + 2.55T_m + 0.0912T_m P \quad (1)$$

This relationship was derived from 113 daily observations representing three dissimilar drainage basins around the globe.

2.2.2 Soil moisture balance

The daily soil moisture budget for the non-irrigated part of the grid cell is given by the original WBM/WTM formulation:

$$dW_s/dt = \begin{cases} -g(W_s)(E_p - P_a) & P_a \leq E_p \\ P_a - E_p & E_p < P_a \leq D_{WS} \\ D_{WS} - E_p & D_{WS} < P_a \end{cases} \quad (2)$$

where $g(W_c)$ is a unitless soil, given by

$$g(W_s) = \frac{1 - e^{(-\alpha \frac{W_s}{W_c})}}{1 - e^{-\alpha}} \quad (3)$$

and W_s [mm] is the soil moisture, E_p [mm d^{-1}] is the potential evapotranspiration, P_a [mm d^{-1}] is the precipitation available for soil moisture recharge (rainfall P_r plus snowmelt M_s), and D_{ws} [mm] is the soil moisture deficit to fill soil to its capacity and satisfy E_p . W_c [mm] is the soil and vegetation-dependent available water capacity and α is an empirical constant (set to 5.0).

2.2.3 Irrigation water demand

The irrigation water demand in the irrigated fraction of the grid cell is computed for individual crops, distributed globally using global data sets of croplands and aggregated crop types (see Sect. 3.2). The approach implemented in WBM_{plus} to estimate crop evapotranspiration for irrigated crops is the crop coefficient method described in FAO's Irrigation and Drainage Paper 56 (Allen et al., 1998) that is widely used to estimate crop water demand at the field scale but was also used at regional (e.g. de Rosnay et al., 2003) and global scale applications (e.g. Döll and Siebert, 2002). This method computes crop evapotranspiration ET_c [mm d^{-1}] as the product of reference evapotranspiration ET_0 [mm d^{-1}] and a crop coefficient k_c . The crop coefficient represents crop physiological parameters and varies with time. A simple soil moisture balance, taking into account precipitation and crop evapotranspiration is kept and irrigation water I_{net} [mm d^{-1}] is applied such that the soil water is refilled to its holding capacity whenever the soil moisture drops below a crop-dependent critical threshold. Rice irrigation is conceptualized by assuming that an additional amount of water is needed to maintain a constant water layer (50 mm) throughout the growing season, and that water percolates out of the root zone at a constant rate into the groundwater. Daily percolation for paddy rice depends on the grid cell soil drainage class (FAO/UNESCO, 2003) and we estimated those rates between 8 mm d^{-1} for "extremely well drained soils" and $2 \text{ [mm d}^{-1}]$ for "very poorly drained soils". The gross irrigation water requirements I_{gr} [mm d^{-1}] (i.e. the amount of water that actually has to be extracted from external water resources) is computed by adjusting the net irrigation demand by the irrigation efficiency E [–] that represents the water losses during irrigation water distribution and the application on the field scale:

$$I_{gr} = \frac{I_{\text{net}}}{E} \quad (4)$$

To determine the onset of the growing season we used agrometeorological conditions (Groten and Ocatre, 2002) based on temperature and precipitation. In the temperate zone, we used a simple temperature threshold and assumed that the growing season starts when the mean monthly air temperature is above 5°C that is frequently used to define the onset of the growing season (Linderholm et al., 2008; Menzel et al., 2003). In regions where crop growth is not limited by temperature we assumed that the growing season starts in the month before the maximum monthly rainfall occurs.

If multiple cropping is possible, the second season is assumed to start 150 days after the first one.

2.3 Runoff retention pool

The excess water X_r [mm d^{-1}] from the vertical water budget (i.e. the sum of the water surplus that is left after evapotranspiration and soil recharge over rain-fed areas and return

flows from irrigated areas) are partially (γX_r) released to the nearby river directly or diverted into the groundwater ($(1-\gamma)X_r$) which is represented as a simple runoff retention pool that delays runoff before it enters the river channel and is described as

$$\frac{dD_r}{dt} = (1-\gamma)X_r - \beta D_r \quad (5)$$

The river runoff becomes

$$R_r = \gamma X_r + \beta D_r \quad (6)$$

where D_r [mm d^{-1}] is the rainfall runoff detention pool, R_r [mm d^{-1}] is the runoff from the grid cell, β is an empirical parameter that controls the outflow from the runoff pool and γ determines the fraction of excess rainfall that fills the pools or becomes runoff instantaneously. The parameter β has units of $1/T$ and has been set to 0.0167, γ is set to 0.5.

It is important to note that WBM_{plus}, like most global water balance models does not account for the dynamics of horizontal groundwater flow or deep groundwater.

2.4 Horizontal water transport

The horizontal water transport in WBM_{plus} is only allowed through river systems. FrAMES offers the basic skeleton for flow routing along gridded river networks that propagates water downstream where the actual flow simulation can be carried out by different methods (Döll and Lehner, 2002; Oki and Sud, 1998; Vörösmarty et al., 2000b). For the present study, we applied a Muskingum-Cunge type solution (Ponce, 1994) of the Saint-Venant flow equations that estimates the outflow Q_{j+1}^{t+1} [$\text{m}^3 \text{ s}^{-1}$] from one grid cell as a linear combination of the inflow Q_j^t and the outflow Q_{j+1}^t from the previous time step and the inflow of the current time step Q_j^{t+1} :

$$Q_{j+1}^{t+1} = C_0 Q_j^{t+1} + C_1 Q_{j+1}^t + C_2 Q_j^t \quad (7)$$

Unit-less coefficients C_0 , C_1 , and C_2 are parameterized based on riverbed geometry considerations. These coefficients can be expressed as a function of the cell Courant number C and cell Reynolds number D :

$$C_0 = \frac{-1 + C + D}{1 + C + D} \quad (8)$$

$$C_1 = \frac{1 + C - D}{1 + C + D} \quad (9)$$

$$C_2 = \frac{1 - C + D}{1 + C + D} \quad (10)$$

which are calculated as:

$$C = U_w \frac{\Delta t}{\Delta l} \quad (11)$$

and

$$D = \frac{Q_m}{W_m S_0 U_w \Delta l}$$

where U_w [$\text{m}^3 \text{s}^{-1}$] is the characteristic speed of the flood wave propagation, Δl [m] is the river cell length, Δt [s] is the time step length, S_0 [–] is the riverbed slope, Q_m [$\text{m}^3 \text{s}^{-1}$] and W_m [m] are mean annual discharge and the corresponding flow width. Considering the Manning or the Chezy flow equation and approximating the riverbed shape with a power-function

$$Y = a W^b \quad (12)$$

where Y [m] and W [m] are the channel depth and with, a is a shape coefficient and b is a shape exponent, the flood wave velocity U_W is strictly a function of the flow velocity U [$\text{m}^3 \text{s}^{-1}$] and the shape exponent b :

$$U_w = U \xi = \left(1 + \frac{bp}{b+1}\right) \quad (13)$$

where p is the exponent of the hydraulic radius according to the Chezy or Manning equations (1/2 or 2/3, respectively). The power function approximation to the riverbed geometry is consistent with empirical in situ discharge-depth and discharge-width relationships (Dingman, 2007). The reference width W_m [m] and depth Y_m [m] at mean discharge Q_m [$\text{m}^3 \text{s}^{-1}$] are calculated by empirical equations:

$$W_m = \tau Q_m^\eta \quad (14)$$

and

$$Y_m = \eta Q_m^\phi \quad (15)$$

where η , τ , v , and ϕ are empirical constants (set to 0.25, 0.40, 8.0, and 0.58, respectively; Knighton, 1998). In the current version of the model, the Muskingum-Cunge parameters C_0 , C_1 , and C_2 are constrained to positive values. If any of the coefficients is negative we set $C_0=1$, $C_1=0$, and $C_2=0$ which is the equivalent of flow accumulation (i.e. routing at infinite flood-wave velocity).

2.5 Reservoirs

Our implementation of reservoir operations distinguishes two kinds of impoundments: (a) “large” reservoirs for river flow control that directly alter the discharge in river channels and (b) “small” reservoirs for local water management that act as an additional storage pool providing water resources for irrigation. Large river flow control reservoirs are represented explicitly by their position in the simulated river network and their impact on discharge is expressed via flow regulation functions that calculate the outflow at the reservoir location as a function of inflow and reservoir storage. Small water management reservoirs are expressed as lumped storage within grid cells that withhold some of the runoff generated on the non-irrigated portion and release it later to supply irrigation water demand.

2.5.1 Large reservoirs

Reservoir operation rules for large scale hydrological models have previously been derived for the main purpose of the reservoir (Haddeland et al., 2006b; Hanasaki et al., 2006). While such an approach is suitable for single reservoirs, applicability on a global scale is a major concern, since the main water management objective for individual reservoirs is not always known and large reservoirs typically serve several purposes. We used a simple relationship of reservoir inflow I_t [$\text{m}^3 \text{s}^{-1}$] and long-term mean inflow I_m [$\text{m}^3 \text{s}^{-1}$] to determine the reservoir release R_t [$\text{m}^3 \text{s}^{-1}$] as

$$R_t = \begin{cases} \kappa I_t & I_t \geq I_m \\ \lambda I_t + (I_m - I_t) & I_t < I_m \end{cases} \quad (16)$$

where κ (set to 0.16) and λ (set to 0.6) are empirical constants that have been found by analyzing operational data from some 30 reservoirs globally. Neglecting evaporation from the reservoir surface, the storage S_t [m^3] in the reservoir can then be described as

$$S_t = S_{t-1} + (I_t - R_t) \Delta t \quad (17)$$

To test the sensitivity of our results with regard to the reservoir release model we performed additional simulations assuming that the release from the reservoir is always equal to the mean annual inflow ($R_t=I_m$) which is the same release model that Hanasaki et al. (2006) used to determine the release from non-irrigation reservoirs.

2.5.2 Small reservoirs

The number of small reservoirs (not counting innumerable small farm ponds) globally could be as high as 800 000 (McCully, 1996). However, given the storage distribution of dams (e.g. Graf, 1999) their combined storage capacity is significantly less than the total installed reservoir volume in large reservoirs. The small reservoirs still play a significant role in providing the water resources needed for irrigation. Small reservoirs intercept local runoff from the non-irrigated areas during the wet season and make it available for irrigation during the cropping period. The storage capacity of such runoff harvesting systems is typically computed with reference to the total irrigation requirement and the amount of runoff available for storage (Srivastava, 2001). WBM_{plus} estimates the total capacity of small reservoirs in each grid cell by accumulating the water required for irrigation and the available surface runoff over one year as

$$C_{sr} = \min\left(\sum \gamma \mu X_r, \sum I_{gr}\right) \quad (18)$$

where μ is a collection factor that describes the fraction of the excess surface runoff that can actually be collected in the reservoirs, and γX_r and I_{gr} are the model estimates of surface runoff (Eq. 6) and irrigation water demand (Eq. 4). The

factor μ depends on a number of local characteristics including topography, land use, geology, and the temporal distribution of rainfall that are not known at the global scale. A design parameter for those systems is the ratio of the area that is needed to collect runoff to supply one unit of irrigated area.

For the present study, we assumed that this fraction must not be greater than 10 based on design recommendations and case studies from a number of regions (Critchley et al., 1991; Srivastava, 1996, 2001). For simplicity, we assumed that small reservoirs in this study have a rectangular cross section and a constant depth of $h=2$ m which is a typical depth of small reservoirs, for example in the semi arid regions of India (Gunnell and Krishnamurthy, 2003; Mialhe et al., 2008). Daily evaporation E [mmd^{-1}] from small reservoirs is computed as $E=\sigma ET_0$, where σ is an evaporation coefficient that has been set to 0.6 (Arnold and Stockle, 1991).

2.6 Irrigation water uptake

The estimated irrigation water withdrawal requirement I_{gr} [mm] can be met (in order) by (1) using locally stored runoff from small reservoirs W_{SR} [mm], (2) by abstracting water from active groundwater (the runoff detention pool D_r) (Eq. 5) W_{GW} [mm], or by (3) abstracting water from local discharge Q_j^t (Eq. 7) (W_{Dis}) [mm], so that the flow in the river is corrected for water abstractions W_{dis} :

$$Q_{j+1}^{t+1} = C_o Q_j^{t+1} + C_1 Q_{j+1}^t + C_2 Q_j^t - W_{dis} \quad (19)$$

In cases where the demand cannot be met by any one of the three sources, water is still supplied at the required rate, by assuming abstractions will be from groundwater systems that are not hydrologically connected to the system (i.e. fossil groundwater resources).

3 Data

3.1 Climate data

Monthly atmospheric forcing data (mean air temperature and precipitation) for the period 1901 to 2002 was obtained from the CRU TS 2.1 data set (Mitchell and Jones, 2005), which represents observed gridded climate data at a spatial resolution of 30 min (longitude \times latitude) and has been widely used for continental and global scale hydrological modeling. This product is not corrected for the effects of errors in gauge-based measurement of precipitation. Significant spatial differences between this product and climate model output data are evident in regions where gauge under catch of solid precipitation and under-representation of precipitation at higher elevations introduce a significant bias on observations (Adam et al., 2006; Tian et al., 2007). Correcting the observed precipitation data sets for those effects could increase the terrestrial precipitation by almost 12% (Adam et al., 2006). The

CRU precipitation data shows an increase in precipitation of 2% globally over the last century (Hulme et al., 1998). Most of the increase in annual precipitation is seen in the northern latitudes, Eastern South America, and Central and Northern Australia. Significant declining trends are observed in Western Africa, Northern Africa, Western South America, and Southern East Asia.

To estimate how uncertainties in precipitation data sets translate to uncertainties in the simulated discharge we performed additional model runs with three well-established global precipitation data sets that are based on observations: (1) the GPCP 1 degree daily data set (Huffman et al. (2001); hereafter GPCP1dd) that uses a suite of satellite data to produce daily precipitation data at 60 min (1deg) spatial resolution, (2) the GPCC monitoring product (Rudolf et al. (2005); hereafter GPCCmon) that interpolated monthly gauging station data at 1 and 2.5 degree spatial resolution, and (3) the VASCLimO monthly data (Beck et al., 2005) that is based on data from around 7000 synoptic stations interpolated to 0.5 degree resolution.

None of these products covers the entire 20th century, and the period covered varies from 1997–present for the GPCP1dd data set, 1986–present for the GPCC monitoring product, and 1951–2000 for the VASCLimO data sets. These data sets differ with respect to the underlying data sources, the correction algorithms, the method of interpolation, as well as the spatial and temporal resolution. The gauge based GPCC and VASCLimO are not corrected for systematic gauge measurement errors.

Considerable differences are therefore evident among those datasets with respect to the spatial and temporal distribution of precipitation on the terrestrial surface. For example, the mean annual precipitation ranges from 99 314 km³ (or 732 mm) for the GPCCmon product to 108 134 km³ (797 mm) for the GPCP1dd product. The respective values for the VASCLimO data sets and the CRU data set are 105 428 km³ (778 mm) and 106 461 km³ (785 mm).

3.1.1 Generating daily precipitation

The non-linearities in system behavior in hydrological processes are particularly relevant with respect to precipitation and the use of monthly or daily precipitation data can lead to significant differences in modeled vertical fluxes (Federer et al., 2003; Vörösmarty et al., 1998). Since the WBM_{plus} model is operated at a daily step, a mechanism was needed to downscale the globally available time series of monthly precipitation inputs to daily values.

We tested two approaches. The first one employed a statistical “weather generator” to create daily rain events by modeling the sequence of wet and dry days within a month based on empirical relationships between monthly rainfall and the number of rainy days and distributing the monthly totals over the wet days such that the daily precipitation amounts follow a gamma distribution (Geng et al., 1986).

The major disadvantage of the weather generator approach was that the spatial correlation of precipitation between neighboring grid cells is “lost” since the daily rain events were generated for each grid cell individually.

The second approach was distributing the monthly values using daily precipitation fractions derived from the GPCP1dd data set. We assumed that the differences in the distribution of daily rainfall between years are small and used the daily rainfall values for the year 2002 to rescale the monthly data for the entire CRU record.

We tested the difference between the two approaches and we found that the resulting differences in model predictions were small. As the second approach leads to a more realistic spatial pattern of precipitation we decided to use the daily fraction derived from the GPGP1dd product.

3.2 Agricultural data sets

To create time-varying data sets of irrigated areas for the last century, we used the University of Frankfurt/FAO Global Map of Irrigated Areas (Siebert et al., 2005a,b) that shows the “areas equipped for irrigation” around the year 2000 at a spatial resolution of 5 arc minutes (around 8 km at the equator) and is based on irrigation statistics from sub-national and national statistics and a variety of atlases and other sources. We rescaled the values in each grid cell on a country-by-country basis using the time series of irrigated areas per country recently compiled from national statistics by Freydanck and Siebert (2008), assuming that the changes in irrigated areas are uniform across each country.

Despite significant uncertainties (in particular for the first half of the last century), and the inability to map changes in the distribution of irrigated areas within a country, this data set adequately reflects the large-scale dynamics of the development of irrigated area over the last century, with an expansion of areas equipped for irrigation from just over 53 Mha in 1901 to 285 Mha in 2002. The four countries India, China, Pakistan, and the US contribute more than 50% of the total irrigated area for the entire period.

It is important to note that not all areas “equipped for irrigation” will actually be irrigated in any given year due to market, conditions, the availability of water, and other local conditions. As the actually irrigated areas are not known for most regions, we assumed that all areas equipped for irrigation were actually irrigated. To model the distribution of crops in irrigated areas, we used the dataset by Monfreda et al. (2008) that shows the distribution of 175 distinct crops across the world in the year 2000 at a spatial resolution of 5 arc minutes and has been derived by synthesizing satellite-derived land cover data and national and international census data. Based on average values of k_c and the length of the growing season, taken from Allen et al. (1998), we aggregated the crops into 4 groups (perennial, vegetables, rice, others), determined average values, and assumed a constant distribution of crops in each irrigated grid cell over the entire

simulation period. Irrigation efficiency data (i.e. the fraction of water actually used by the crop related to the water abstracted from sources) has been taken from the country averaged numbers provided by AQUASTAT (2008) and Döll and Siebert (2002). Irrigation intensity (defined as the total area of harvested crops over the total irrigated area) was derived from AQUASTAT (2008). Soil hydraulic properties to determine the soil moisture holding capacity in both, non-irrigated and irrigated fractions of the grid cell have been taken from the UNESCO/FAO soil map of the world (FAO/UNESCO, 2003).

All data sets have been regridded to 30 min resolution.

3.3 Hydrography data

3.3.1 River network

To link the terrestrial land mass to the oceans and to route the modeled runoff, we used the Simulated Topological Network (STN) of gridded rivers at 30-min spatial resolution (Vörösmarty et al., 2000a,b) that organizes the terrestrial land mass of the continents into 6192 river basins with catchment size ranging from 10^3 to 5.9×10^6 km².

3.3.2 Reservoirs

River flow regulating (“large”) reservoirs are represented as points along the simulated gridded network where WBM_{plus} applies simple reservoir operation rules (Sect. 2.4) to simulate water release from the reservoir. Location and attributes of the existing reservoirs were taken from the global repository of registered impoundments (Vörösmarty et al., 1997, 2003) that reports reservoirs with a maximum storage capacity of more than 0.5 km³ and contains 668 reservoirs from the International Commission on Large Dams (ICOLD) registry of dams (ICOLD, 1998, 2003). The combined contemporary maximum capacity for those reservoirs was 4726 km³ and represents 67% of the total volume of impoundments formed by dams with a height of more than 15 m. Reservoirs were co-registered to the STN-30 river network ensuring that reservoirs are located on main tributaries. Reservoirs sharing the same grid cell were collapsed into single reservoir with the sum of capacities of the individual reservoirs. The year of construction given in the ICOLD database was used to create a time-varying data set of reservoir capacities.

4 Model simulations

4.1 20th century simulations

Model simulations for the last century were performed for two different configurations. First, we computed the components of the hydrological cycle under natural conditions, i.e. the reservoir and the irrigation water modules were turned off. The second configuration simulated disturbed conditions using the time varying agricultural data sets described above

to estimate irrigation water demand and water withdrawals plus the reservoir routing for any existing reservoirs.

We did not account for the interactions of atmospheric CO₂ concentrations with the hydrological cycle through reduced transpiration per unit leaf and thus increasing runoff assuming total leaf area is unchanged (Betts et al., 2007). Furthermore, we did not investigate the effects of land use changes (most notably deforestation) that have been shown to have significant impacts on the hydrological cycle (Gordon et al., 2005; Haddeland et al., 2007; Piao et al., 2007) and have been shown to increase runoff globally (Piao et al., 2007) at the same order of magnitude as the changes imposed by increased evapotranspiration in irrigated areas (Gordon et al., 2005). We do not consider the contribution of thawing permafrost and melting of glaciers on continental runoff.

Daily potential evapotranspiration was computed using the Hamon relationship (Hamon, 1963) as a function of daily mean air temperature and the length of the day and taken as reference evapotranspiration ET₀[mm] to compute crop water demand in irrigated areas:

$$ET_0 = \frac{715.5 \Lambda e_s T_m}{T_m + 273.2} \quad (20)$$

Where $\Lambda[-]$ is the daylength (expressed as a fraction of a 24 h period), and e_s [kPa] is the saturation water pressure at the mean air temperature T_m [°C]. Vörösmarty (1998) used 11 commonly used evapotranspiration functions for a water balance model applied to the conterminous US and found that runoff estimates produced using the Hamon function had the lowest bias of all tested reference evapotranspiration functions when compared to observed values. Similar findings have been reported by Oudin et al. (2005) who tested a set of 27 evapotranspiration functions over a large set of catchments around the globe and concluded that simple temperature dependent function produce the best results with regard to model efficiency and found no advantage in using more complex methods.

It is important to note that in keeping with earlier approaches (Federer et al., 2003; Vörösmarty et al., 1998) the model parameters in the WBM_{plus} model were assigned a priori and not further calibrated to match observed discharge.

4.2 Sensitivity analysis

We used a Generalised Likelihood Uncertainty Estimation (GLUE, Beven and Binley, 1992; Freer et al., 1996) approach to test the impact of variations in the model parameters on predicted discharge. This approach is aimed at investigating prediction uncertainty and parameter sensitivity by randomly sampling the parameters within a predefined range and performing a large number of model simulations. Clearly, such an approach is not applicable at the global domain so it was applied for example river basins.

As the sensitivity of model parameters is correlated with hydroclimatic conditions (Demaria et al., 2007; van Werkhoven et al., 2008) we applied the method to the Danube river basin (station Cetail Izmail; A=788 000 km²) and the Mississippi river basin (gauging station Vicksburg; A=2964252 km²) for the period 1995 to 1999.

5 Results and discussion

5.1 Model validation

Previous versions of the WBM/WTM model were validated against discharge records in various geographical regions (e.g. conterminous US by Vörösmarty, 1998; Amazon by Vörösmarty, 1996 and globally by Fekete, 2002). All previous studies showed that WBM/WTM had little bias (<4% on annual average observed runoff when applied to the conterminous US) over large domains while individual basins could have large discrepancies. For the present study we validated predicted monthly time series of simulated discharge against the same set of discharge gauges from the Global Runoff Data Centre (GRDC) that was used in previous work in developing UNH-GRDC Composite Runoff Fields (Fekete et al., 2002, 1999). The selected 663 stations monitor 52% of the continental land mass (excluding Antarctica) and 70% of the continental discharge to oceans (Fekete et al., 2002). The period of observation varies greatly between stations with a peak in data availability in the 1980's. We further reduced the number of stations by including only those stations that have a minimum length of record of 10 years. The number of observation-months for the final selection of 660 stations ranges from 120 to 1224 (mean 541, median 477) months. Model performance was assessed using the Mean Bias Error (MBE), computed as the sum of the differences of predicted values P_i minus observed values O_i divided by the number of observations, the mean absolute error (MAE), computed as the sum of the absolute differences between P_i and O_i over the number of observations, and the Index of agreement d (Willmott, 1981), given by:

$$d = 1 - \frac{\sum_{i=1}^n (O_i - P_i)^2}{\sum_{i=1}^n (|P_i - \bar{O}| + |O_i - \bar{O}|)^2} \quad (21)$$

that ranges from zero for a model that is not a better predictor than the mean observed value to 1.0 for a perfect model.

Figure 1 shows the frequency distribution of the mean monthly bias and the d-statistics for the selected stations for model simulations under disturbed conditions from 1901–2002. Despite significant differences between simulated and observed discharge at some gauging stations, the low bias reaffirms our findings regarding WBM's low bias when applied over large spatial domains. Averaged for all stations, the average MBE of $-1.2 \text{ mm month}^{-1}$ indicates that the

model on average underestimates discharge and this negative bias can partly be explained with biases arising from errors in the precipitation input fields due to gauge undercatch (Sect. 3.1.1). As the bias arising from uncertainties in the input data partly cancels out over large domains, the model performance generally increases with basin size (Fekete et al., 2002; Hunger and Döll, 2008). In basins with one or more registered reservoirs ($n=219$), the model performance increases slightly when the model run is performed under disturbed conditions (d increase from 0.684 to 0.694) and the coefficient of variation (CV) of monthly discharge decreases from 1.2 under natural conditions to 1.1 under disturbed conditions (compared to an observed CV of 0.97). As the area under irrigation represents less than 1% of the catchment area for the majority of the basins, changes in model performance will not be seen for most basins but are significant individual river basins (Sect. 5.3.3).

The sensitivity analysis for model parameters revealed that discharge predictions are most sensitive to variations in the parameters γ that effectively separates runoff into a slow and a fast component, and SF that partitions precipitation to rainfall and snowfall, although the impact of variations in SF, β , and γ on annual values of predicted discharge is minimal.

We selected the 0.05 and 0.95 percentiles of the likelihood weighted discharge values at each time step based on the d-statistics using the GLUE approach. The resulting GLUE prediction bounds for the “best” 1000 out of 5000 simulations with varying parameters are shown in Fig. 2.

On average, the range in discharge predictions represents 23% of the mean simulated discharge using the original parameters. To put these results into perspective, we also plotted the predicted discharge using three additional precipitation data sets. These variations are much larger than the parameter uncertainty and confirm the results of Biemans et al. (2009) who compared the impact of precipitation uncertainty on simulated discharge on 294 river basins globally and found an average discharge uncertainty of 90%.

The results of the Mississippi river basin (data not shown) revealed a very similar pattern with regard to the range of uncertainty of parameters and input data and show that, although mostly ignored, uncertainty in discharge predictions on continental and global scales is governed by uncertainty in precipitation data sets (Biemans et al., 2009).

5.1.1 Irrigation water withdrawal

The simulated amount of water that needs to be abstracted from groundwater, small reservoirs, and rivers globally based on the time-varying data set of irrigated areas described above increased from $590 \text{ km}^3 \text{ a}^{-1}$ in 1901 to $2997 \text{ km}^3 \text{ a}^{-1}$ for the year 2002.

The estimate of the contemporary withdrawal is consistent with previous estimates based on the same contemporary distribution of irrigated areas that range from $2200 \text{ km}^3 \text{ a}^{-1}$ to around $3000 \text{ km}^3 \text{ a}^{-1}$ (Döll and Siebert, 2002; Hanasaki

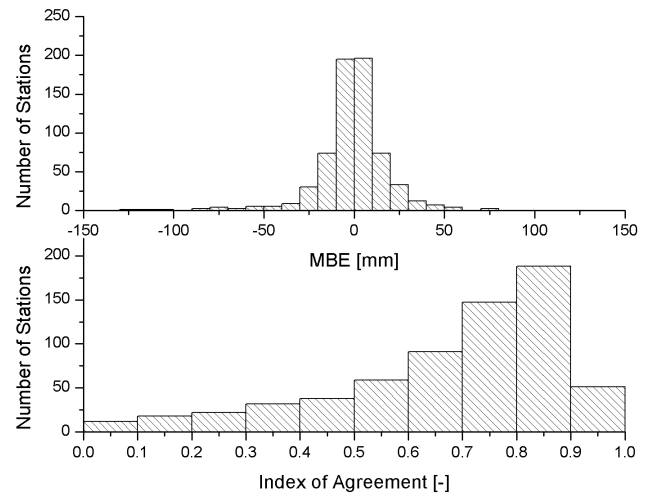


Fig. 1. Frequency distribution of the mean model bias for the selected 660 gauging stations. Average MBE is $-1.2 \text{ mm month}^{-1}$, average Index of Agreement, d , 0.68.

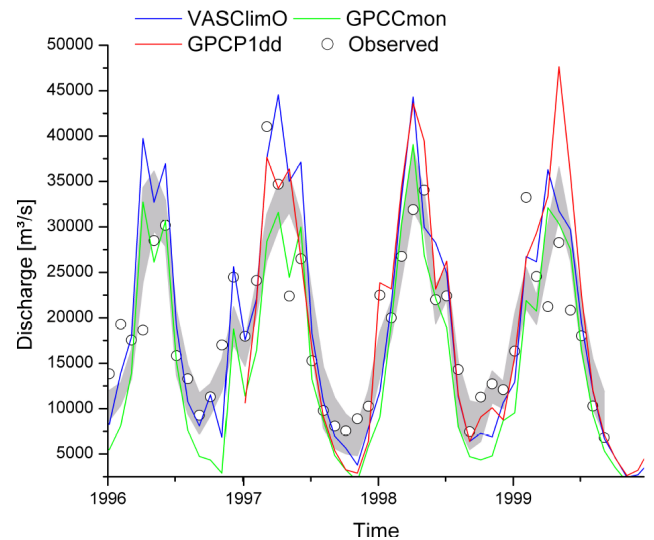


Fig. 2. GLUE estimated uncertainty in the predicted discharge for the Mississippi river basin based on 1000 selected simulations (grey), observed values (circles) and model simulations for three different precipitation data sets.

et al., 2008; Siebert and Döll, 2007; Vörösmarty et al., 2005). By continents, most of the withdrawal is estimated for Asia ($\sim 83\%$), home to most of the worlds rice paddies and multiple cropping (Maclean et al., 2002). Irrigation water withdrawal in North America ($\sim 6\%$ of the total) increased sharply between 1940 and 1950 (Fig. 3). With the exception of Europe ($\sim 3\%$ of the global withdrawal), all continents show a steady upward trend over the last 100 years in irrigation water use reflecting the expansion of irrigated areas (Sect. 3.2).

As the withdrawal of water for irrigation will have different impacts on components of the hydrological cycle, as well as biogeochemical fluxes, depending on the source where it is taken from, it is important to know if the water is supplied by groundwater or surface water. Although some estimates exist on the global scale, a detailed, consistent inventory of this information is lacking (Oki and Kanae, 2006). The fraction of irrigation that is supplied by groundwater varies greatly within regions. US agriculture, for example, relies on 65% groundwater (Pimentel et al., 2004), while groundwater is supplying an estimated 50% to 60% in India (Singh and Singh, 2002; Thenkabail et al., 2006), and 40% in China (Thenkabail et al., 2006). Foster and Chilton (2003) compiled data on irrigation water use for selected countries and concluded that the contribution of groundwater to irrigation water abstractions is approaching 30% globally.

The WBM_{plus} computed estimates for the contribution of discharge from rivers and the runoff detention pool D_r are 10% and 17%, respectively and 33% being supplied from locally stored runoff in small reservoirs (Table 1). As noted earlier, cases can occur where the demand cannot be met by either locally produced runoff or river corridor discharge, representing the mining of fossil groundwater. Our estimates of the volume of water that has to be abstracted from those non-renewable sources increased from $220 \text{ km}^3 \text{ a}^{-1}$ in 1901 to $1200 \text{ km}^3 \text{ a}^{-1}$ under contemporary conditions, representing 40% of the estimated global agricultural water withdrawal. While this estimate is consistent with earlier estimates of the unsustainable water use (Rost et al., 2008; Vörösmarty et al., 2005), it may represent an overestimation as WBM_{plus} does not represent the dynamics of large groundwater systems from which water can be withdrawn in areas far away from the areas where the system is recharged. This lack of an adequate representation of deeper groundwater is a key shortcoming of current macroscale hydrology models (Lettenmaier, 2001). Over the last century, the total accumulated volume of non-renewable water abstractions is $55\,639 \text{ km}^3 \text{ a}^{-1}$, representing about half of the total precipitation reaching the Earth's surface in one year. The total water withdrawn from non-renewable water resources represents only about 0.2% the volume of water currently stored in all groundwater stocks, estimated to be $23 \times 10^6 \text{ km}^3$ (Oki and Kanae, 2006).

5.2 Spatial trends in hydrological components

To assess spatial patterns of trends in predicted components of the hydrological cycle over the last century, we computed trends of the predicted annual values of evapotranspiration and runoff for each grid cell under natural and disturbed conditions. Under natural conditions, the spatial distribution of the trend in simulated evapotranspiration over the last century reflects the variations in the temperature and precipitation drivers (Fig. 4).

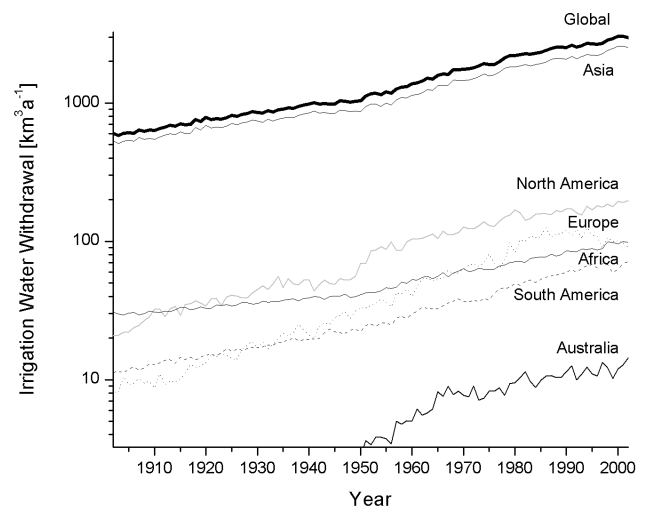


Fig. 3. Time series of modeled irrigation water withdrawal over the last century aggregated by continents.

Table 1. Modeled water withdrawal from different sources under contemporary conditions.

Water source	Water withdrawal [$\text{km}^3 \text{ a}^{-1}$]	Percentage of total withdrawal
Small Reservoirs	989	33
Local groundwater	509	17
River discharge	300	10
Non-renewable sources	1199	40
Global total	2997	100

As the temperature shows an upward trend for almost all regions, the trends in evapotranspiration for individual continents are dominated by increases or decreases in available water and hence by the increases or decreases in the precipitation data. Increases in evapotranspiration are seen in the mid to high latitude regions, Central Southern Africa, Eastern South America, and Central Australia.

Under disturbed conditions, the expansion of irrigated areas over the last century has significantly increased evapotranspiration in Eastern China, the India, Central America, and Central Asia. Negative trends in predicted evapotranspiration reflect the changes in precipitation and can be seen in Western and Central Africa, Western South America, and parts of South East China.

Predicted changes in evapotranspiration and trends in the precipitation input data result in increases in the predicted natural runoff (precipitation – evapotranspiration) in the high latitude regions, Eastern South America, Northern Australia, and mid-latitude North America and runoff decreases in Western Africa, Argentina, Eastern China, and parts of Central Asia (Fig. 5).

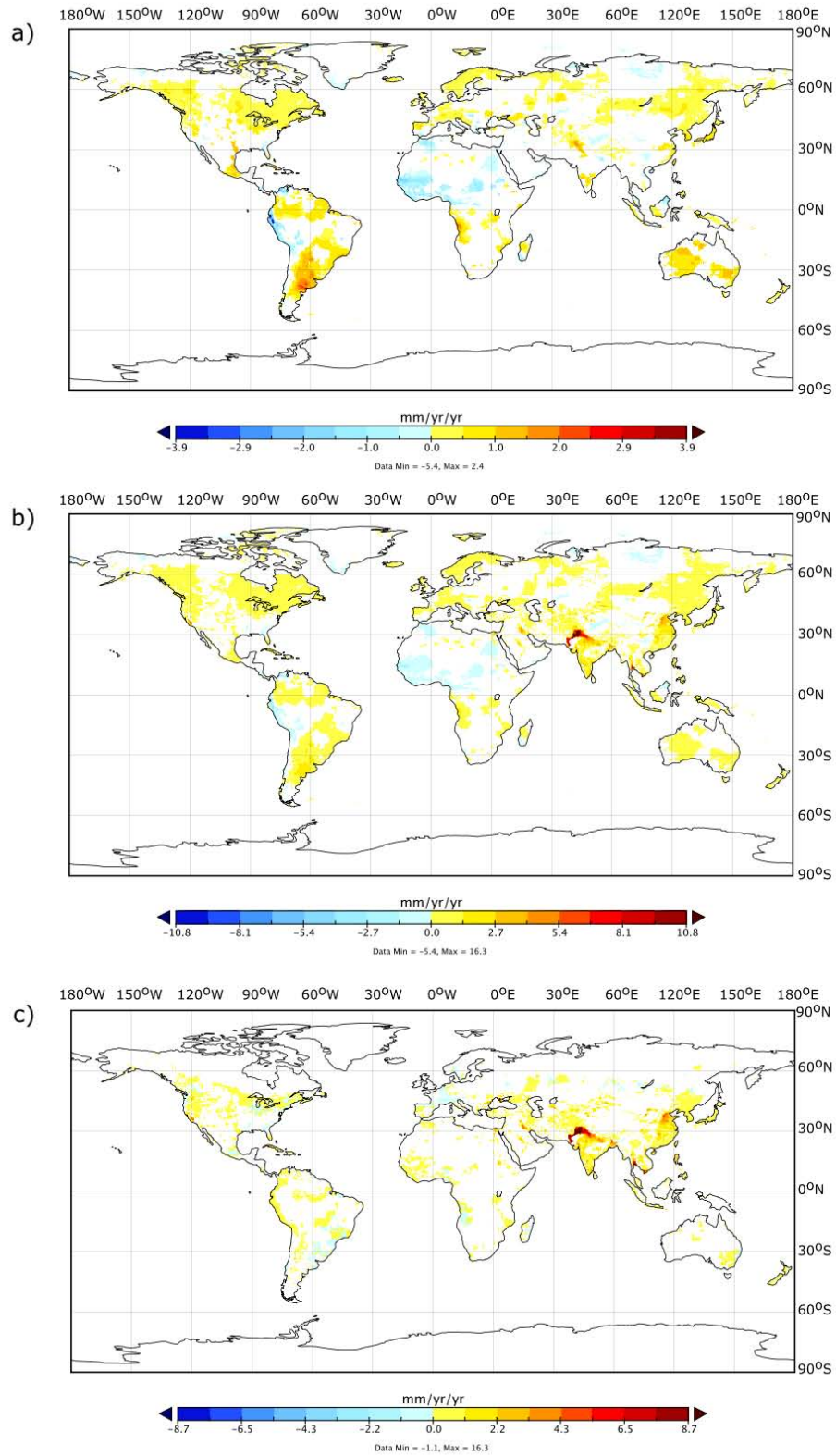


Fig. 4. Significant trends [mm a^{-2}] in modeled annual values of evapotranspiration for (a) natural, (b) disturbed conditions and (c) differences in significant trends between disturbed and natural conditions for the period 1901–2002. Trends were tested for significance at the 5% level.

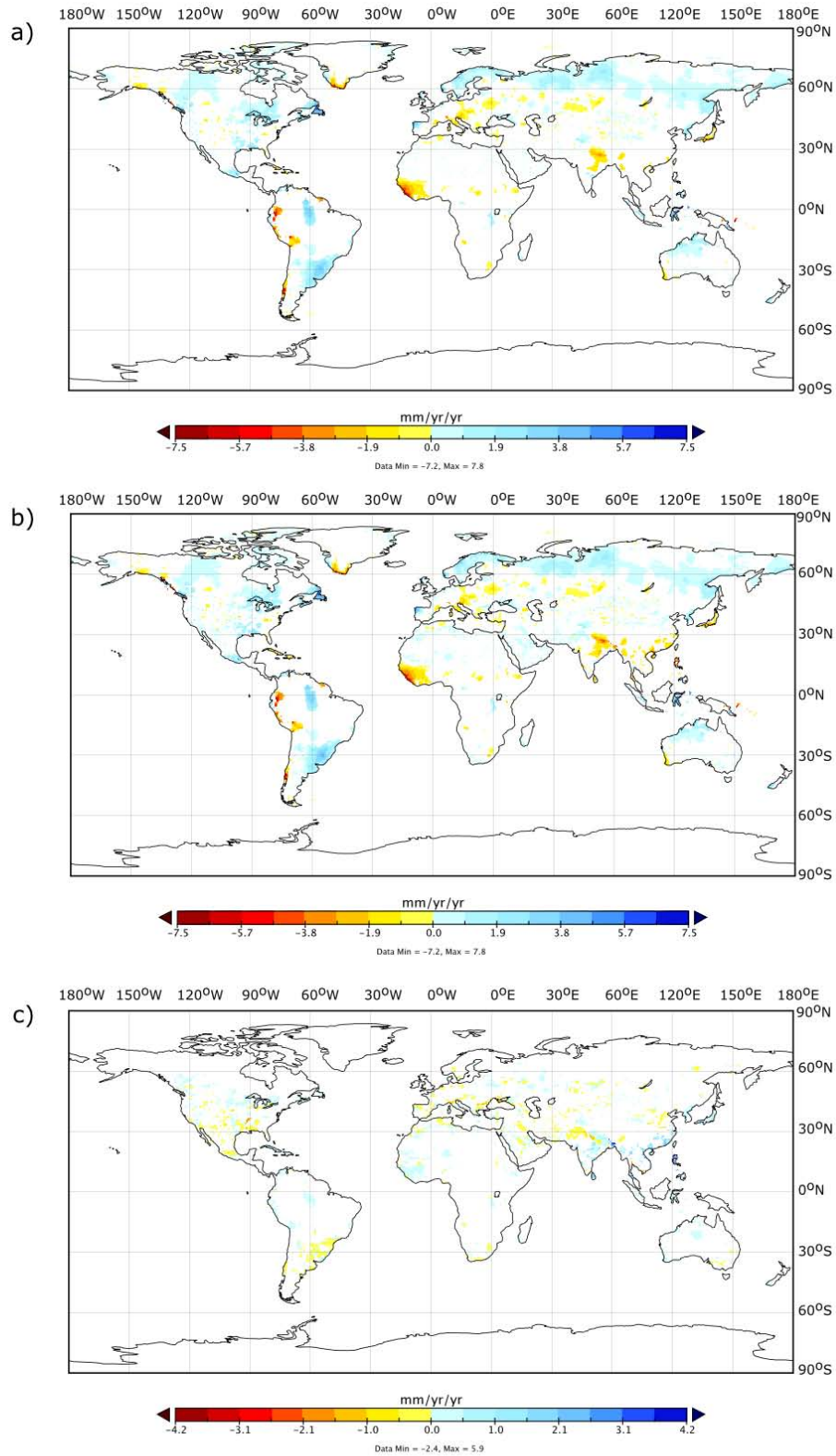


Fig. 5. Significant trends [mm a^{-2}] in modeled annual values of runoff for (a) natural, (b) disturbed conditions and (c) differences in significant trends between natural and disturbed conditions for the period 1901–2002. Small increases in runoff in dry regions under disturbed conditions are caused by return flows from irrigated areas. Trends were tested for significance at the 5% level.

The general pattern of the spatial distribution of runoff trends is consistent with the global distribution of significant trends in observed discharge for the period 1971–1998 compared to 1901 to 1970 (Milly et al., 2005; Milliman et al., 2008) and observed increases in North America (e.g. Qian et al., 2007). Changes in evapotranspiration imposed by the expansion of irrigated areas and increased evapotranspiration translate to significant decreases in the predicted runoff in Eastern China and India.

5.3 Global discharge

The changes in the climate drivers alone – increased evapotranspiration due to irrigation, and the changes in groundwater storage and reservoir operation translate to changes in the predicted terrestrial discharge into the oceans and to endorheic basin receiving waters (e.g. Aral and Caspian Seas). Based on the basin characteristics given in the STN river network (Sect. 3.3.1; Fig. 6) we calculated time series of flow water entering the oceans and endorheic basins and determined the significance of possible trends in those time series at the 0.05 level.

This section will first discuss the total predicted terrestrial discharge over the last century and then the predicted discharge for individual oceans and from continents reflecting the impact of variations in the climate drivers alone and from changes induced by the expansion of irrigated lands and the operation of reservoirs (Fig. 7).

The results are compared with earlier estimates by Fekete et al. (2002) that have been derived by combining modeled runoff with observed discharge at 663 river gauging stations and simulated discharge using three additional global precipitation data sets. Annual time series of discharge in major endorheic rivers and major rivers draining into the ocean basins for the last century are shown in Fig. 8.

Our estimate of the long term mean annual freshwater export from the terrestrial surface of the Earth (taking into account irrigation water abstractions) for the last century is $37\,401\text{ km}^3\text{ a}^{-1}$ and is consistent with earlier estimates that range between $35\,400$ and $39\,300\text{ km}^3\text{ a}^{-1}$ (Dai and Trenberth, 2002; Döll et al., 2003; Fekete et al., 2002; Sitch et al., 2003; Vörösmarty et al., 2000c, 2005)

The estimated annual discharge varies considerably between $32\,783$ and $41\,725\text{ km}^3\text{ a}^{-1}$, a larger range than estimates made by Shiklomanov and Rodda (2003) and shows the highest values during the period 1951–1975 (Table 2). The highest value of annual terrestrial discharge ($41\,725\text{ km}^3\text{ a}^{-1}$) is $\sim 12\%$ higher than the long-term mean annual value. The minimum annual discharge (in 1992) in the last century is 16% lower than the mean annual value and is related to the substantial decrease in global precipitation following the eruption of Mt. Pinatubo in June 1991 (Trenberth and Dai, 2007). Over the entire simulation period, the global total runoff increases slightly ($11\text{ km}^3\text{ a}^{-1}$ under natural conditions and $6\text{ km}^3\text{ a}^{-1}$ when the effects of water

abstractions for irrigation are taken into account) but both trends are not significant. The flow alteration imposed by the construction of reservoirs over the last century gradually decreased the variability of the estimated discharge expressed by the coefficient of variation (CV) of monthly discharge values and is discussed in more detail in Sect. 5.5.

The increased evapotranspiration over irrigated areas leads to a reduction of terrestrial runoff that is partly offset by the additional water abstracted from groundwater systems that are not connected to the hydrological cycle (Sect. 5.1.1). Combined, this additional water and increased evapotranspiration leads to a gradual reduction of global discharge ranging from 0.6% at the beginning of the last century to around 2% in 2000.

Variations in precipitation input translate to changes in the long-term mean terrestrial discharge between -11% (using GPCComon data) and $+2\%$ using GPCP1dd data (Table 2 and Fig. 7).

Despite being insignificant for the total discharge entering the oceans, the hydrologic alterations imposed by the construction of reservoirs and the expansion of irrigated areas may have dramatic effects at the regional scale and thus impact the flow to the oceans or endorheic receiving waters. Table 3 summarizes the characteristics of basins draining into the oceans and irrigated areas and an overview of the basins and the receiving oceans is given in Fig. 6.

5.3.1 Land/endorheic basins

Major internally draining basins include the Central Asian Drainage basin, the Caspian Sea, the Aral Sea, and major endorheic lakes in Africa. Around 1.45% of the area in those basins is equipped for irrigation and the installed reservoir capacity, expressed as the mean residence time (reservoir capacity over mean annual discharge) is 0.29 (under contemporary conditions).

The estimated annual discharge from those basins shows considerable variations (between $774\text{ km}^3\text{ a}^{-1}$ and $1650\text{ km}^3\text{ a}^{-1}$ under disturbed conditions) and is $1037\text{ km}^3\text{ a}^{-1}$ on average (Table 2). Discharge in endorheic basins is slightly declining over the entire period, most notably in the last 25 years in of the last century. Over the last century, the trend is negative (but insignificant), $-0.2\text{ km}^3\text{ a}^{-1}$ under natural conditions and $-0.5\text{ km}^3\text{ a}^{-1}$ taking into account the effects of irrigation water withdrawal.

The construction of reservoirs has lead to a considerable decrease of the variability of monthly flows, most drastically in the period 1975–2000, where the coefficient of variation (CV) for monthly discharge has increased from 0.52 to 0.37 (Table 2). Figure 8 shows the modeled time series for the Okavango river with high flows during the 1970's that was followed by a series of dry years in the mid 1980's.

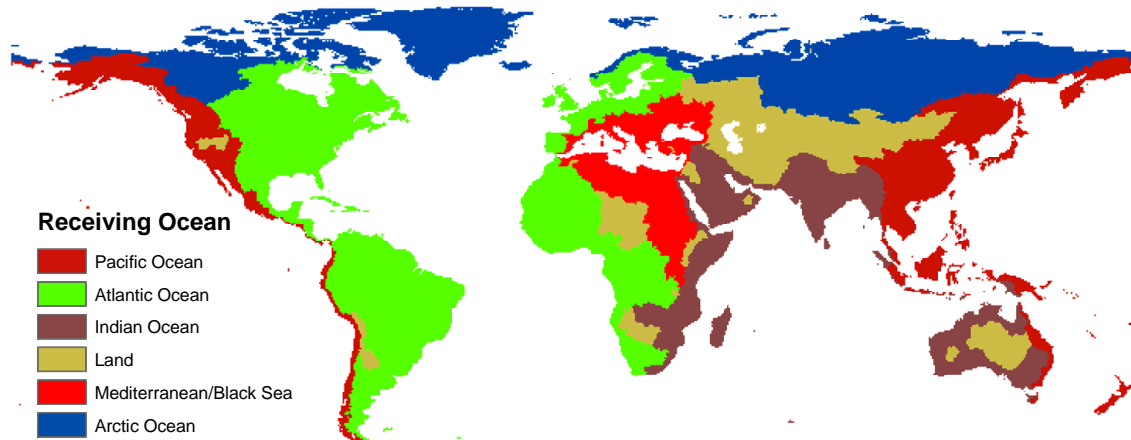


Fig. 6. Overview of river basins and receiving oceans, based on the STN-30 river network.

Table 2. Components of the hydrological cycle for endorheic basins and basins draining into the oceans. Fluxes in $\text{km}^3 \text{a}^{-1}$. Coefficient of variation (CV) calculated from monthly flows. nat.: model run under natural conditions, dist: model results under disturbed conditions (irrigation water abstractions and reservoir operation turned on) P =precipitation, ET =evapotranspiration, Q =discharge. L=Land, M+BS=Mediterranean/Black Sea, ArO=Arctic Ocean, PO=Pacific Ocean, IO=Indian Ocean.

Ocean		1901/1925		1926/1950		1951/1975		1976/2002		1901/2002		VASCLimO	GPCP1dd	GPCPmon	Fekete 2002
		nat	dist	nat	dist	nat	dist	nat	dist	nat	dist	1951–2000	1997–2007	1986–2007	climatology
L	P	5799		5728		5949		5917		5849		6010	6771	5644	
	ET	4718	4764	4652	4713	4793	4893	4863	5012	4752	4849	4940	5427	4811	
	Q	1060	1040	1062	1033	1137	1097	1032	984	1072	1037	1066	1354	842	993
	CV	0.51	0.51	0.5	0.49	0.51	0.42	0.52	0.37	0.51	0.45	0.48	0.62	0.46	
M+BS	P	4922		4912		5003		4777		4901		4893	5112	4619	
	ET	3887	3720	3688	3728	3707	3765	3657	3752	3684	3742	3760	3853	3650	
	Q	1205	1188	1213	1191	1280	1236	1098	1066	1197	1168	1134	1250	962	1205
	CV	0.28	0.28	0.29	0.29	0.27	0.27	0.29	0.34	0.29	0.3	0.33	0.49	0.41	
ArO	P	7613		7809		8083		8018		7884		6647	9326	7309	
	ET	4445	4446	4615	4616	4561	4562	4612	4614	4559	4561	4539	4853	4444	
	Q	2101	2101	2185	2185	2480	2462	2379	2375	2288	2282	2092	3943	2333	3268
	CV	1.03	1.03	0.96	0.96	1.01	0.97	1	0.93	1	0.97	1.10	1.15	1.08	
PO	P	21641		21857		22394		21827		21928		21790	21543	20199	
	ET	11979	12166	12086	12327	12020	12388	12182	12734	12069	12410	12130	12099	11644	
	Q	9666	9518	9746	9564	10357	10095	9658	9350	9853	9626	9634	9457	8547.3	10476
	CV	0.19	0.19	0.19	0.19	0.2	0.18	0.19	0.17	0.2	0.18	0.21	0.26	0.23	
AO	P	50215		50166		51072		50931		50602		50261	50359	47167	
	ET	32129	32153	32117	32150	32275	32330	32660	32742	32302	32352	32913	32185	30797	
	Q	18106	18088	18084	18060	18825	18778	18344	18296	18340	18305	17325	18179	16374	18507
	CV	0.23	0.23	0.24	0.23	0.23	0.22	0.26	0.24	0.24	0.23	0.26	0.29	0.29	
IO	P	15109		15204		15579		15294		15296		15827	15021	14376	
	ET	9925	1025	9869	10292	10048	10612	10193	11063	10012	10566	10290	10429	9846	
	Q	5133	4953	5274	5059 5477	5196	5065	4742	5234	4983	5525	4589	4522	4858	4858
	CV	0.33	0.3	0.34	0.31	0.33	0.29	0.33	0.3	0.33	0.3	0.39	0.33	0.33	
Total	P	105298		105675		108081		106764		106461		105428	108134	99314	
	ET	67083	68274	67027	67826	67404	68550	68167	69917	67378	68480	68572	68846	65192	
	Q	37271	36888	37564	37092	39556	38864	37576	36813	37984	37401	36776	38772	33580	39307
	CV	0.19	0.19	0.2	0.19	0.19	0.18	0.21	0.18	0.2	0.19	0.21	0.25	0.21	

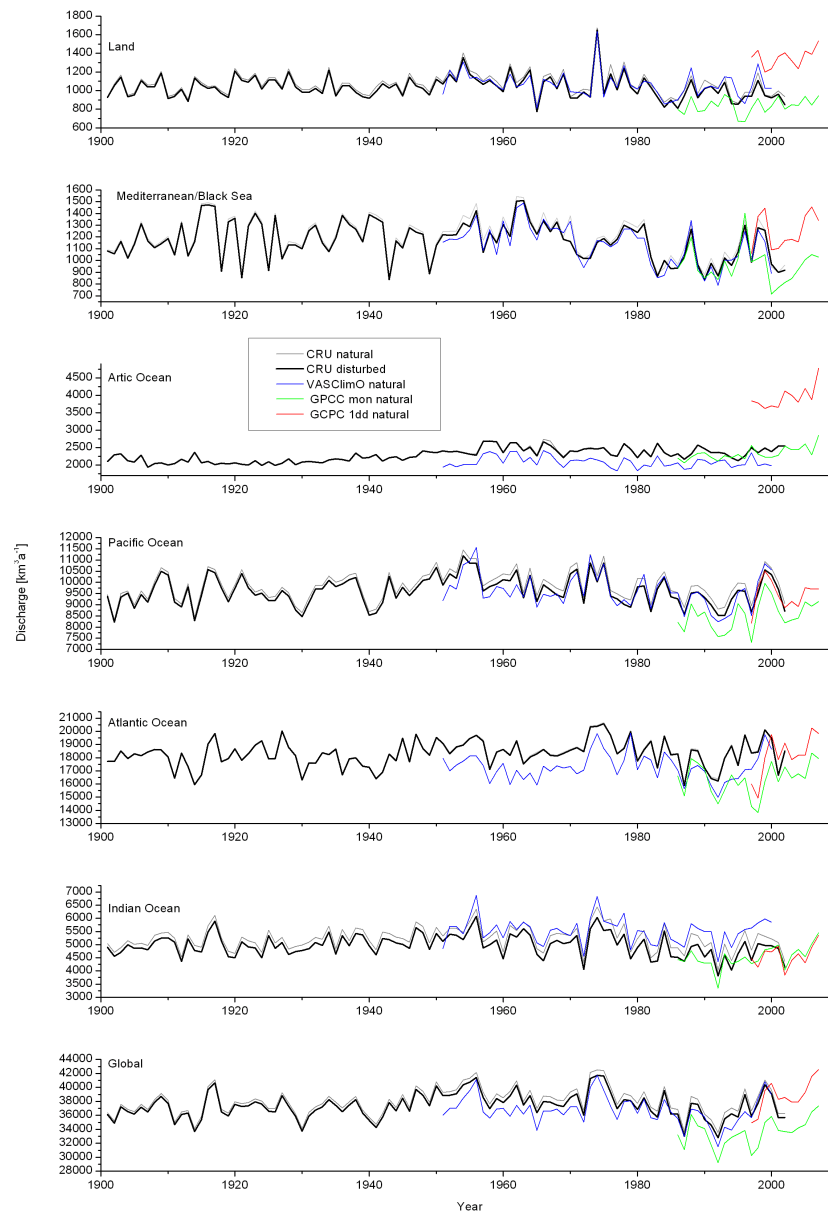


Fig. 7. Annual time series of modeled discharge to the ocean and to endorheic basins under natural (gray line) and disturbed (black line) conditions 1901–2002. Land refers to internally draining (Central Asian Drainage basin, Caspian Sea, Aral Sea, and major endorheic lakes in Africa). Additional model results using different precipitation data sets indicate the uncertainties in the discharge to the oceans as a result of uncertainties in precipitation data sets GPCPC 1dd (red), VASCLimO (blue) GPCPC mon (green) under natural conditions.

5.3.2 Ocean receiving waters

Mediterranean/Black Sea

The basins draining into the Mediterranean and Black Sea are among the most heavily influenced with regard to the effects of irrigation and reservoirs (Table 3). The discharge to the Black Sea is dominated by the Danube (50%), the Dnepr (15%) and the Don (9%).

The discharge to the Mediterranean is dominated by the flow of the river Nile contributing more than 53% to the total inflow. Other important rivers include the Po (9%) and the Rhone river (7%). Similar to endorheic basins, basins draining into the Mediterranean are experiencing a decline in discharge in the last 25 years of the last century. Over the last century, the trend in discharge under natural conditions is $-1.2 \text{ km}^3 \text{ a}^{-1}$ (significant) and under disturbed conditions $-1.4 \text{ km}^3 \text{ a}^{-1}$ (insignificant).

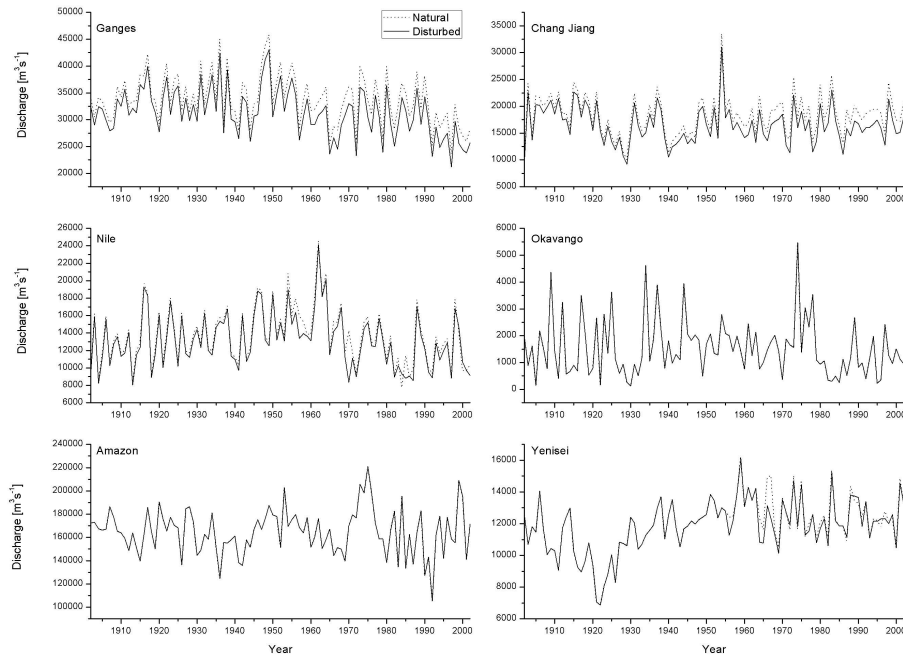


Fig. 8. Annual time series of modeled river discharge (at river mouth) under natural and disturbed conditions (1901–2002) for major rivers in different ocean basins: Ganges (Indian Ocean), Nile (Mediterranean), Amazon (Atlantic Ocean), Chang Jiang (Pacific Ocean), Okavango (Internal basin), and Yenesei (Arctic Ocean).

Table 3. Characteristics of endorheic basins and basins draining into the oceans and computed trends in modeled annual discharge 1901–2002 (significant trends in bold). Irrigated areas and reservoir capacities based on 2002 data. Residence time is computed as total reservoir volume over mean annual runoff; taken from Fekete et al. (2002). Basin delineation based on the STN-30 river network.

Ocean	Area [km ²]	Reservoir Capacity [km ³]	Irrigated Area [km ²]	Irrigated Area [%]	Residence Time [a]	Trend (natural) [km ³ a ⁻²]	Trend (disturbed) [km ³ a ⁻²]
Land	18 743 062	290	271 121	1.45	0.29	-0.21	-0.54
Mediterranean/Black Sea	10 678 622	506	233 241	2.18	0.42	-1.19	-1.41
Atlantic Ocean	45 729 720	1904	362 296	0.79	0.10	5.84	5.41
Indian Ocean	20 688 590	611	927 762	4.48	0.13	-0.14	-2.07
Pacific Ocean	19 931 492	742	826 268	4.15	0.07	2.71	0.51
Arctic Ocean	19 824 778	673	12 472	0.06	0.21	4.25	4.13
Global	135 596 264	4726	2 633 160	1.94	0.12	11.27	6.02

It is important to note, that our modeled discharge under disturbed conditions can be higher than the estimated discharge under natural conditions in very dry years, for example in 1984 and 2000 (Fig. 7).

This can largely be explained with the irrigation in grid cells along the Nile river and in the Nile delta that do not fall in the same grid cell as the river and therefore cannot be supplied by river discharge. As the local runoff in these regions is close to zero, water is primarily supplied from

fossil groundwater sources and the return flow from irrigated areas eventually increases runoff (Abderrahman, 2005; Al-Weshah, 2000; Wheida and Verhoeven, 2006).

Atlantic Ocean

About 30% of the terrestrial flow to the Atlantic Ocean is coming from the Amazon river. Other important rivers include the Zaire (9%), Mississippi (4%), and Parana (4%).

Given the large volume of discharge entering the Atlantic Ocean, the effect of human interventions on the discharge volume is negligible small; over the last century, the combined effect of increased evapotranspiration and water withdrawal from non-renewable sources reduces the annual discharge into the Atlantic Ocean by $33 \text{ km}^3 \text{ a}^{-1}$ (0.2%). The annual flow of the Amazon river shows considerable variations but is not affected by irrigation water abstractions (Fig. 8).

Over the last century, discharge into the Atlantic Oceans shows an upward (but insignificant) trend of $5.4 \text{ km}^3 \text{ a}^{-1}$ and $5.8 \text{ km}^3 \text{ a}^{-1}$ under natural conditions and disturbed conditions, respectively.

Indian Ocean

The most important rivers draining into the Indian Ocean are the Ganges (with a flow equivalent to 23% of the total), the Irrawaddy (12%), and the Zambezi (6%). Our estimate of the long-term mean annual discharge entering the Indian Ocean is $4983 \text{ km}^3 \text{ a}^{-1}$ with significant reductions imposed by the expansion of irrigated areas and increased evapotranspiration in basins draining into the Indian Ocean. With 4% of the drainage area being under irrigation, irrigation water abstraction reduces the total flow to the Indian Ocean by almost 5% averaged over the last century with a reduction reaching the highest values ($\sim 7\%$) in the last 25 years of the 20th century. Under both disturbed and natural conditions, the time series show decreasing but insignificant trends ($-0.14 \text{ km}^3 \text{ a}^{-1}$ and $-2.0 \text{ km}^3 \text{ a}^{-1}$). Figure 8 illustrates the gradual reduction of discharge under natural and disturbed conditions over the last century for the Ganges river.

Pacific Ocean

Important rivers draining to the Pacific Ocean include the Chang Jiang (9%), the Mekong (4%) and the Amur (3%). Although areas under irrigation represent $\sim 4\%$ of the drainage area (Table 3), increased evapotranspiration translates only to a reduction of $341 \text{ km}^3 \text{ a}^{-1}$ representing 2.3% of the discharge under natural conditions (averaged over the entire simulation period). With the expansion of irrigated areas, the reduction of flow gradually increases, with a steep increase in the last half of the last century. The long-term discharge under disturbed conditions ($9626 \text{ km}^3 \text{ a}^{-1}$) varies considerably over the last century. As with discharge into the Atlantic, discharge was highest in the 1951–1975 period ($\sim 5\%$ higher than averaged over the 20th century). Over the entire simulation period, discharge under natural and disturbed conditions increases by $2.7 \text{ km}^3 \text{ a}^{-1}$ and $0.5 \text{ km}^3 \text{ a}^{-1}$, respectively, both trends being insignificant. Flow reductions in the Chang Jiang river basin are depicted in Fig. 8.

Arctic Ocean

Flow into the Arctic Ocean is dominated by the Yenisei (17%), Ob (13%), Lena (10%), Mackenzie (7%), and Dvina (4%) rivers contributing to more than half of the total flow. Owing to the large volumes of spring discharge that is dominated by snow melt compared to summer flows, the variability of streamflow entering the Arctic Ocean is higher than for any other ocean (CV for monthly values under natural conditions is around 1.0). Reservoirs are responsible for a substantial change in the seasonality of streamflow in Arctic river basins (Adam et al., 2007), and the construction of reservoirs over the last century has gradually led to a slight reduction of the variability of modeled discharge entering the Arctic Ocean (Table 2). It is noteworthy that our estimate of the long-term mean annual discharge into the Arctic Ocean ($2282 \text{ km}^3 \text{ a}^{-1}$) is around 30% lower than the $3268 \text{ km}^3 \text{ a}^{-1}$ estimated from gauge corrected runoff fields (Fekete et al., 2002) and the $3200 \text{ km}^3 \text{ a}^{-1}$ estimated based on contemporary discharge records (Serreze et al., 2006). The discrepancy can largely be attributed the huge uncertainties in Arctic hydroclimatological data arising from the sparse network of Arctic climate stations (see Sect. 5.3.3).

Also, as WBM_{plus} neglects glaciers and permafrost, these processes could partly explain the differences between modeled and observed values.

Over the last century, we find that discharge into the Arctic Ocean shows a significant positive trend of $4.2 \text{ km}^3 \text{ a}^{-1}$. This trend is consistent with the annual rate of increase of $2.0/+2.7 \text{ km}^3 \text{ a}^{-1}$ that has been estimated from observed discharge from the six Eurasian Arctic rivers from 1936–1999 (Peterson et al., 2002) and upward trend of $8.2 \text{ km}^3 \text{ a}^{-1}$ for the period 1949–2004 that has been found by Dai et al. (2009) from a new dataset of observed streamflow where missing data were filled by results from simulations of a land surface model.

5.3.3 Uncertainties in discharge to oceans

As discussed earlier, large uncertainties are associated with the predicted discharge entering the oceans. These uncertainties can mostly be attributed to uncertainties in the gridded fields of precipitation and gauge under catch, due to the vicinity of gauge locations to highly populated places (Rawlins et al., 2006) and the non-representativeness of those gauges of complex topographic features (Adam et al., 2006).

The range in predicted discharge entering the Arctic ocean therefore varies considerably; compared to CRU based prediction, GPCP1dd discharge is 72% higher whereas VASCLimO data results in discharge that is 12% lower than the long-term CRU based discharge (Fig. 7 and Table 2). For endorheic basins, the GPCP1dd predictions are 30% lower,

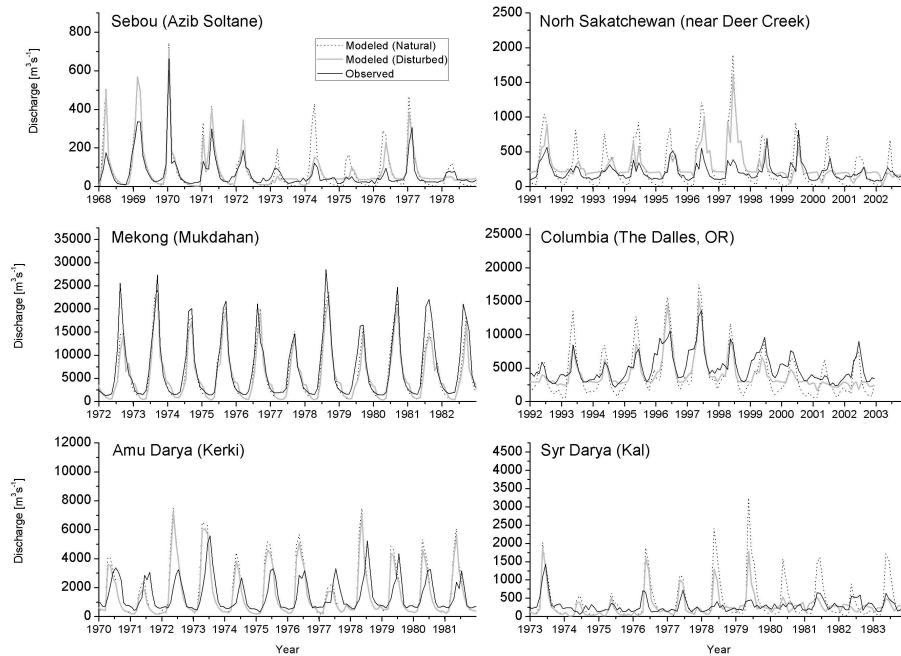


Fig. 9. Observed and simulated river discharge (under natural and disturbed) conditions for selected gauging stations.

whereas GPCPmon predictions are 17% lower than those based on CRU. For other ocean basins, the differences are less pronounced and are less than 20%.

5.4 Model results for selected river basins

This section is aimed at discussing the simulated discharge at selected river basins and exemplifying the impact of irrigation water management and reservoir operation on simulated monthly hydrographs.

Figure 9 shows time series of monthly values (aggregated from daily predictions) of observed and modeled time series under natural and disturbed conditions for selected gauging stations representing a wide range of catchment sizes, water management practices and climatic conditions.

Syr Darya and Amu Darya, feeding the Aral Sea in Central Asia are among the most prominent examples of heavily impacted river basins. The two basins have undergone significant distortions of their hydrographs due to the expansion of irrigated areas and the construction of reservoirs in the 1960's and 1970's. The abstraction of water for irrigation purposes has led to the shrinking of the Aral Sea to about half its size and to a reduction of about 90% of its volume (Micklin, 2007).

Two reservoirs were constructed upstream of the station at Kal at the Syr Darya river in the tributaries Naryan river and Kara Narya River in 1978 and 1980 with a combined storage capacity of 21.75 km³. As a result, the hydrograph shows a significant decrease in the variability. The coefficient of

variation (CV) for modeled monthly values of discharge for the pre-management period (1950–1969) decreased from 1.2 to 0.52 for the period 1980–1999, and is closer to the CV of observed values (0.44) for the same period.

Similarly, irrigation water use reduces the estimated flow in the Amu Darya at Kerki by 14% and the operation of reservoirs lead to an increase in low flows whereas flows during the wet season are greatly reduced. It is important to note that discharge in the Syr Darya is overpredicted for both natural and disturbed conditions. One of the reasons is a significant loss of water (through evaporation and seepage) in both rivers during their passage through the desert that is currently not considered in the model. Nezhlin et al. (2004) estimated that these losses amount to 30% of the flow.

The Sebou river, one of the largest rivers in Morocco is heavily influenced by the development of irrigation with natural vegetation covering only 25% of the total catchment area of 40 000 km² (Snoussi, 2002). The construction of the Idriss Ier dam on the Inaouene tributary in 1973 ($V=1270$ km³) has led to a remarkable decrease in the variability of the observed flow and a reduction of the total flow of about 55% (Snoussi et al., 2002). While the model simulations under natural conditions for the gauging station at Azib Soltane capture the observed hydrograph reasonably well, the natural simulations after the construction of the reservoir grossly overestimate the variability and volume of the flow, indicating that the operation of reservoirs need to be taken into account to adequately represent the anthropogenic changes in macroscale hydrological models.

Despite a large storage capacity of reservoirs upstream of the gauging station at Mukdahan (8.46 km^3), the seasonality of the flow of the Mekong river is not significantly affected by the operation of reservoirs (Haddeland et al., 2006a). The consumptive use for the total area is $8.2 \text{ km}^3 \text{ a}^{-1}$ and represents a 4% decrease in streamflow, comparable to the previous estimates of water withdrawal for the entire basin of $13 \text{ km}^3 \text{ a}^{-1}$ (Haddeland et al., 2006a).

Being one of the most heavily regulated river basins in North America with a combined storage capacity of 76 km^3 in the area upstream of the gauging station “The Dalles”, reservoir operation and irrigation depletion have greatly affected the river flow of the Columbia River. The variability of monthly modeled discharge decreased from 0.82 for the first half of the century to 0.46 for the period after 1950 (compared to observed values of 0.70 and 0.43). Water abstraction for irrigation has lowered the flow volume by 2.5% on average during the same period.

The flow volume of the North Saskatchewan near “Deer Creek” is unaffected by irrigation water use but significantly altered by the construction of two reservoirs with a combined capacity of 2.5 km^3 . Variability of monthly flows decreased from around 1.0 in the period before 1970 to 0.52 for period after 1970 and captures the variability of observed streamflow (0.56) during the same period reasonably well despite differences in the modeled flow volume.

5.5 River water aging

Vörösmarty et al. (1997) introduced the concept of river water aging, related to residency time change of river flow through artificial impoundments, to illustrate the impact of the construction of reservoirs on simulated discharge over the last century. It must not be confused with the true “age” of water molecules that can be determined, for example, using tracer hydrological methods.

We apply here this concept and compute the mean water age of water entering the oceans and endorheic basins under natural and disturbed conditions. The aging of water in its passage to the oceans reflects disturbance in the natural water cycle and determines a number of direct and indirect changes in the physical, biogeochemical, and geomorphological processes, such as hydrograph distortion, re-aeration capacity, sediment trapping efficiency (Vörösmarty and Sahagian, 2000).

Building on earlier work by Vörösmarty et al. (1997) and using the river bed parameterization described in equations described in Sect. 2.4, we can estimate the natural and reservoir-induced residence time τ_m [s] of water in each grid cell. Residence time is determined by relating the modeled annual discharge Q_m [m^3/s] to the river volume V_{riv} [m^3] and reservoir volume V_{res} (accumulated downstream using the STN-30 network):

$$\tau_m = \frac{uV_{\text{res}} + V_{\text{riv}}}{Q_m} \quad (22)$$

where u is a utilization factor that relates mean modeled annual storage in each reservoir to the reservoir capacity and V_{riv} is the storage volume in the river, computed as $V_{\text{riv}} = Y_m W_m$ (Eqs. 14 and 15). The computed age varies with the modeled annual discharge and the estimated reservoir storage based on the reservoir operation described in Sect. 2.5.1. Our estimate of the discharge weighted apparent water age globally is 19 days and is consistent with earlier estimates (Covich, 1993; Vörösmarty et al., 2000b, 1997). The discharge weighted age of water entering the oceans varies considerably between 8 days for basins entering the Pacific Ocean and 39 days for the Mediterranean basins (Table 4).

The additional water age imposed by the construction of impoundments in the last century has increased the mean water age by 42 days, with the largest increases in $\Delta\tau_m$ observed in endorheic basins, basins draining to the Mediterranean and basins draining into the Pacific Ocean. The differences in the apparent aging under natural and disturbed conditions are depicted in Fig. 10.

The apparent additional aging $\Delta\tau_m$ shows the most significant increase during the period 1950–1980 when the construction of large reservoirs has reached its peak and flattens out after the 1980’s (Fig. 11).

Assuming that the release from the reservoir is equal to the long-term mean annual flow (see Sect. 2.5.1) did not significantly impact these estimates; the global mean water age under disturbed conditions increased to 64 days and the increases for individual oceans in the apparent additional aging $\Delta\tau_m$ was less than 10%.

These changes have a number of direct and indirect effects on the temporal distribution of discharge, biogeochemical processes in the river and geomorphologic process. For example, the construction of reservoirs has been shown to result in significant losses in sediments in the coastal zone (Vörösmarty et al., 2007, 2003) and thereby influences the effective sea level rise in a number of highly populated deltas, including the Nile, Ebro, Volta, and Niger (Vörösmarty et al., 2007).

6 Summary and conclusions

Using a water balance and transport model with time series of climate drivers we have reconstructed the hydrography of terrestrial discharge for the last century, explicitly accounting for the effects of human interventions in the hydrological cycle. To separate the effects of human engineering and the climate drivers alone, model simulations were performed for disturbed and natural conditions. The good agreement between observed and predicted discharge at a large number of gauging stations globally (Fig. 1) indicates that the model simulations, forced with time-varying geospatial data sets of irrigated areas and reservoirs reproduces the variations in components of the hydrological cycle caused by the

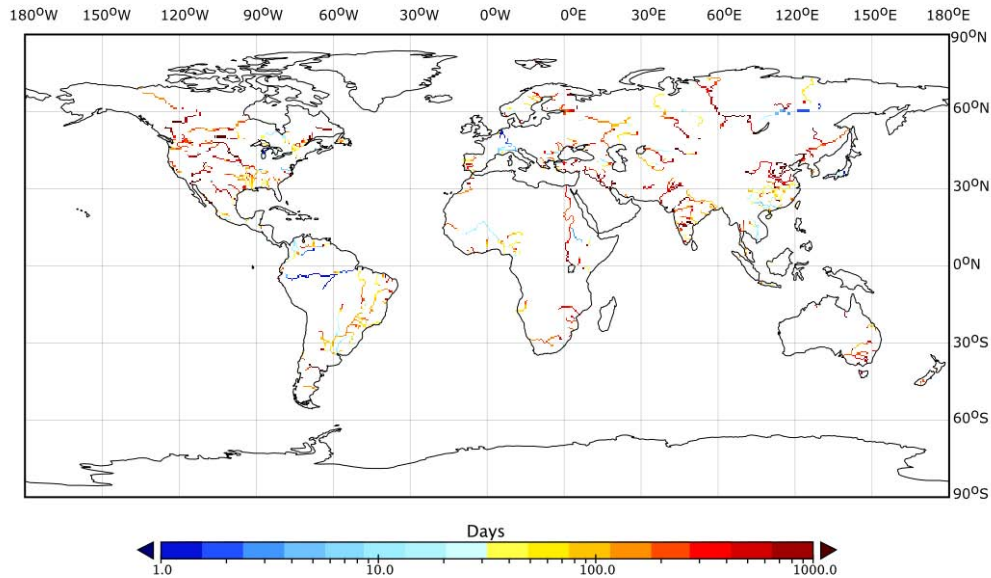


Fig. 10. Differences in the apparent aging of water in major rivers under natural and disturbed conditions for the contemporary population of reservoirs.

Table 4. River storage volume and apparent age of water entering the Oceans and endorheic basins.

Ocean	V_{riv} [km ³]	τ_m (natural) [d]	τ_m (2002) [d]	$\Delta\tau_m$ [d]
Pacific	192	8	38	30
Atlantic	1143	24	56	32
Indian	142	12	57	45
Land	50	20	143	123
Mediterranean	105	39	205	166
Arctic	133	24	112	88
Total	1765	19	61	42

climate drivers and the anthropogenic changes reasonably well. The approach can therefore potentially be used to help understanding the role of human interventions in continental and global water cycles for near-real time predictions and future scenarios of those drivers.

The results for individual river basins suggest a reduction of flow as a result of the expansion of irrigation and changes in the seasonality of flow imposed by the operation of reservoirs. These results are in general agreement with previous observations (Bouwer et al., 2006; Haddeland et al., 2006b) and highlight the need to account for human interventions in the water cycle in macroscale hydrological models. The changes in the hydrological cycle in river basins with a large fraction of the basin area under irrigation have been shown to be governed by the impact of human engineering rather than changes in the climate signal. Despite dramatic impacts

in individual river basins, the annual discharge entering the oceans is governed by variations in the climate forcings over the last century and is not significantly altered by water abstractions for irrigation (Dai et al., 2009; Milliman et al., 2008).

Under natural conditions, we find significant decreasing trends ($-1.2 \text{ km}^3 \text{ a}^{-1}$) of the flows entering the Mediterranean and Black Sea and significantly increasing discharge ($4.2 \text{ km}^3 \text{ a}^{-1}$) to the Arctic Ocean.

With the exception of the Arctic Ocean, we do not find significant increasing trends in modeled time series of accumulated streamflow entering the major ocean basins and endorheic receiving waters over the last century, consistent with previous reports (Dai et al., 2009; Milliman et al., 2008) and contradicting the notion of increasing global runoff as a result of global warming (Labat et al., 2004).

The construction of large reservoirs over the last century has gradually and significantly altered the seasonality of streamflow and the dynamics of horizontal water transport in the network of rivers. Using the water aging concept as an indicator to describe the impact of reservoirs on the horizontal transport we found a 300% increase of the apparent water age that, in turn, impacts a number of biogeochemical, geomorphological, and physical processes.

Our estimates of components of the hydrological cycle under natural and disturbed conditions are constrained by a number of uncertainties in the input data as well as uncertainties related to the model itself.

We also recognize the difficulties in separating the effects of changes in the hydrological cycle caused by natural and anthropogenic factors using the simple method presented here because of the interrelated links among climate,

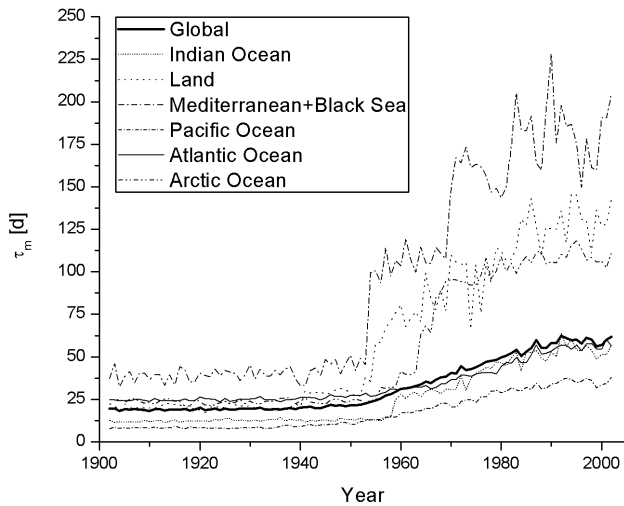


Fig. 11. Time series of the discharge weighted apparent water age for discharge entering the oceans and endorheic basins.

atmosphere, soil, and vegetation dynamics (Piao et al., 2007). For example, it is possible that irrigated areas deliver an additional amount of precipitation (Moore and Rojstaczer, 2001) so that the observed rainfall already contains an anthropogenic signal.

With regard to the distortion of hydrographs due to the operation of reservoirs, our results are constrained by the incomplete global repository of registered reservoirs (Vörösmarty and Sahagian, 2000). Although the dataset of large reservoirs represents an estimated 67% of the total storage volume of impoundments formed by dams over 15 m, river flow is significantly impacted by the operation of smaller reservoirs that are not accounted for in our model but collectively have a significant impact on river flow and sediment retention (Vörösmarty et al., 2003). Presumably, such uncertainties will gradually be reduced with the development of more accurate, consistent and comprehensive global inventories of dams and reservoirs in combination with high resolution global river networks that are only emerging (Lehner et al., 2008). With regard to the estimated fraction of the water supplied from non-renewable sources, uncertainties arise from an inadequate representation of large groundwater systems and the lack of a global repository of inter-basin water transfers. Uncertainties in the distribution of irrigated areas are related to the area that is actually irrigated in given year (as opposed to the area equipped for irrigation that is reported in the Global Map of Irrigated areas). Globally, this area is estimated to represent 72% of the area equipped for irrigation (Siebert and Döll, 2007). However, these area estimates are much lower than estimates based on remotely sensed data. For example, a recently prepared new data set of global irrigated areas (Thenkabail et al., 2006) exceeds previous estimates by 40% (Wisser et al., 2008). The implications of differences in the estimates of irrigated areas

can be quite dramatic; globally, the estimated irrigation water demand can vary by $\sim 30\%$ but variations for individual countries are larger.

The significance of uncertainties in precipitation on a global-scale water balance context has been previously shown (Biemans et al., 2009; Fekete et al., 2004). As could be shown, the uncertainties in the precipitation datasets typically translate to higher relative errors in runoff in semiarid regions and the use of different precipitation data sets may therefore lead to different spatial and temporal trends in the hydrological variables. These uncertainties are typically ignored in calibration strategies for macro scale hydrological models and can possibly lead to wrong parameter estimates and calibration results (Biemans et al., 2009). As shown here, the uncertainty related to precipitation exceeds the uncertainty related to model parameters.

Future versions of the modeling approach will minimize some of the uncertainties related to data sets by using different physical data sets of climate drivers (temperature, precipitation) and data related to human interventions (irrigated areas, reservoirs) as they become available.

Acknowledgements. Observed discharge data has been provided by the Global Runoff Data Centre (GRDC) in Koblenz, Germany. We thank N. Hanasaki for providing operational reservoir data. Funding was provided by the NASA Applied Earth Sciences Program through Cooperative Agreement NNA06CN09A, the NASA IDS program (NNX07AH32G), and the NASA Terrestrial Hydrology Program (NNX07AW08G). The presented simulations are part of the Global Terrestrial Network for Hydrology (GTN-H) effort by the World Meteorological Organization that is an effort to establish water cycle monitoring capabilities. The results, together with a number of supplementary model predictions (both historically and near-real time) and data products are available to the scientific community through the GTN-H website (<http://www.gtn-h.net>). Supplementary figure is available at <http://www.hydrol-earth-syst-sci.net/14/1/2010/hess-14-1-2010-supplement.pdf>

Edited by: T. Wagener

References

- Abderrahman, W. A.: Groundwater management for sustainable development of urban and rural areas in extremely arid regions: A case study, *Int. J. Water Resour. Dev.*, 21, 403–412, 2005.
- Adam, J. C., Clark, E. A., Lettenmaier, D. P., and Wood, E. F.: Correction of global precipitation products for orographic effects, *J. Climate*, 19, 15–38, 2006.
- Adam, J. C., Haddeland, I., Su, F., and Lettenmaier, D. P.: Simulation of reservoir influences on annual and seasonal streamflow changes for the Lena, Yenisei, and Ob' rivers, *J. Geophys. Res.-Atmos.*, 112, D24114, doi:10.1029/2007JD008525, 2007.
- Al-Weshah, R. A.: Optimal use of irrigation water in the Jordan Valley: A case study, *Water Resour. Manag.*, 14, 327–338, 2000.

- Allen, R. G., Pereira, L. S., Raes, D., and Smith, M.: Crop Evapotranspiration: guidelines for computing crop water requirements, Food and Agricultural Organization of the United Nations (FAO), 1998.
- Arnold, J. G. and Stockle, C. O.: Simulation of supplemental irrigation from on-farm ponds, *J. Irrig. Drain. E.-ASCE*, 117, 408–424, 1991.
- Beck, C., Grieser, J., and Rudolf, B.: A New Monthly Precipitation Climatology for the Global Land Areas for the Period 1951 to 2000, Deutscher Wetterdienst (DWD), Offenbach, Germany, 181–190, 2005.
- Betts, R. A., Boucher, O., Collins, M., Cox, P. M., Falloon, P. D., Gedney, N., Hemming, D. L., Huntingford, C., Jones, C. D., Sexton, D. M. H., and Webb, M. J.: Projected increase in continental runoff due to plant responses to increasing carbon dioxide, *Nature*, 448, 1037–U1035, doi:10.1038/nature06045, 2007.
- Beven, K. and Binley, A.: The future of distributed model: model calibration and uncertainty prediction, *Hydrol. Process.*, 6, 279–298, 1992.
- Biemans, H., Hutjes, R. W. A., Kabat, P., Strengers, B., Gerten, D., and Rost, S.: Impacts of precipitation uncertainty on discharge calculations for main river basins, *J. Hydrometeorol.*, 10(4), 1011–1025, doi:10.1175/2008JHM1067.1, 2009.
- Bouwer, L. M., Aerts, J. C. J. H., Droogers, P., and Dolman, A. J.: Detecting the long-term impacts from climate variability and increasing water consumption on runoff in the Krishna river basin (India), *Hydrol. Earth Syst. Sci.*, 10, 703–713, 2006, <http://www.hydrol-earth-syst-sci.net/10/703/2006/>.
- Covich, A. P.: Water and Ecosystems, in: *Water in crisis*, edited by: Gleick, P. H., Oxford University Press, UK, 504 pp., 1993.
- Critchley, W., Siebert, K., and Chapman, C.: *Water harvesting. A manual for the design and construction of water harvesting schemes*, FAO, Rome, Italy, 1991.
- Dai, A. G. and Trenberth, K. E.: Estimates of freshwater discharge from continents: Latitudinal and seasonal variations, *J. Hydrometeorol.*, 3, 660–687, 2002.
- Dai, A. G., Qian, T. T., Trenberth, K. E., and Milliman, J. D.: Changes in Continental Freshwater Discharge from 1948 to 2004, *J. Climate*, 22, 2773–2792, 2009.
- de Rosnay, P., Polcher, J., Laval, K., and Sabre, M.: Integrated parameterization of irrigation in the land surface model ORCHIDEE. Validation over Indian Peninsula, *Geophys. Res. Lett.*, 30, 1986 pp., doi:10.1029/2003GL018024, 2003.
- Demaria, E. M., Nijssen, B., and Wagener, T.: Monte Carlo sensitivity analysis of land surface parameters using the Variable Infiltration Capacity model, *J. Geophys. Res.-Atmos.*, 112, D11113, doi:10.1029/2006JD007534, 2007.
- Dickonson, R. E., Zebiak, S. E., Anderson, J. L., Blackmon, M. L., Luca, C. D., Hogan, T. F., Iredell, M., Ji, M., Rood, R. B., Suarez, M. J., and Taylor, K. E.: How can we advance our weather and climate model as a community?, *B. Am. Meteorol. Soc.*, 83, 431–434, 2002.
- Dingman, L. S.: Analytical derivation of at-a-station hydraulic geometry relations, *J. Hydrol.*, 334, 17–27, 2007.
- Döll, P. and Lehner, B.: Validation of a new global 30-min drainage direction map, *J. Hydrol.*, 258, 214–231, 2002.
- Döll, P. and Siebert, S.: Global modeling of irrigation water requirements, *Water Resour. Res.*, 38, 1037 pp., doi:10.1029/2001WR000355, 2002.
- Döll, P., Kaspar, F., and Lehner, B.: A global hydrological model for deriving water availability indicators: model tuning and validation, *J. Hydrol.*, 270, 105–134, 2003.
- Federer, C. A., Vörösmarty, C., and Fekete, B.: Sensitivity of annual evaporation to soil and root properties in two models of contrasting complexity, *J. Hydrometeorol.*, 4, 1276–1290, 2003.
- Fekete, B. M., Vörösmarty, C. J., and Grabs, W.: Global, Composite Runoff Fields based on Observed river discharge and simulated water balances, Global Runoff Data Centre (GRDC), Report 22, 1999.
- Fekete, B. M., Vörösmarty, C. J., and Grabs, W.: High-resolution fields of global runoff combining observed river discharge and simulated water balances, *Global Biogeochem. Cy.*, 16, 1042 PP., doi:10.1029/1999GB001254, 2002.
- Fekete, B. M., Vörösmarty, C. J., Roads, J. O., and Willmott, C. J.: Uncertainties in precipitation and their impacts on runoff estimates, *J. Climate*, 17, 294–304, 2004.
- Foster, S. S. D. and Chilton, P. J.: Groundwater: the processes and global significance of aquifer degradation, *Philos. T. R. Soc. B*, 358, 1957–1972, 2003.
- Freer, J., Beven, K., and Ambroise, B.: Bayesian Estimation of Uncertainty in Runoff Prediction and the Value of Data: An Application of the GLUE Approach, *Water Resour. Res.*, 32, 2161–2173, 1996.
- Freydank, K. and Siebert, S.: Towards mapping the extent of irrigation in the last century: time series of irrigated area per country, Insititue of Physical Geography, University of Frankfurt, Frankfurt am Main, Germany, Frankfurt Hydrology Paper 08, 2008.
- Galy-Lacaux, C., Delmas, R., Kouadio, G., Richard, S., and Gosse, P.: Long-term greenhouse gas emissions from hydroelectric reservoirs in tropical forest regions, *Global. Biogeochem. Cy.*, 13, 503–518, 1999.
- Geng, S., de Fries, F. W. T. P., and Supit, I.: A simple method for generating daily rainfall data, *Agr. Forest. Meteorol.*, 36, 363–376, 1986.
- Ghassemi, F. and White, I.: *Inter-basin water transfer: case studies from Australia, United States, Canada, China, and India*, International Hydrology Series, Cambridge University Press, UK, 462 pp., 2007.
- Gordon, L. J., Steffen, W., Jonsson, B. F., Folke, C., Falkenmark, M., and Johannessen, A.: Human modification of global water vapor flows from the land surface, *Proc. Natl. Acad. Sci. USA.*, 102, 7612–7617, 2005.
- Graf, W. L.: Dam nation: A geographic census of American dams and their large-scale hydrologic impacts, *Water Resour. Res.*, 35, 1305–1311, 1999.
- Groten, S. M. E. and Ocatre, R.: Monitoring the length of the growing season with NOAA, *Int. J. Remote. Sens.*, 23, 2797–2815, 2002.
- Gunnell, Y. and Krishnamurthy, A.: Past and present status of runoff harvesting systems in dryland peninsular India: A critical review, *Ambio*, 32, 320–324, 2003.
- Haddeland, I., Lettenmaier, D. P., and Skaugen, T.: Effects of irrigation on the water and energy balances of the Colorado and Mekong river basins, *J. Hydrol.*, 324, 210–223, 2006a.
- Haddeland, I., Skaugen, T., and Lettenmaier, D. P.: Anthropogenic impacts on continental surface water fluxes, *Geophys. Res. Lett.*, 33, L08406, doi:10.1029/2006GL026047, 2006b.

- Haddeland, I., Skaugen, T., and Lettenmaier, D. P.: Hydrologic effects of land and water management in North America and Asia: 1700–1992, *Hydrol. Earth Syst. Sci.*, 11, 1035–1045, 2007, <http://www.hydrol-earth-syst-sci.net/11/1035/2007/>.
- Hamon, W. R.: Computation of direct runoff amounts from storm rainfall, *Int. Assoc. Sci. Hydrol. Publ.*, 63, 52–62, 1963.
- Hanasaki, N., Kanae, S., and Oki, T.: A reservoir operation scheme for global river routing models, *J. Hydrol.*, 327, 22–41, 2006.
- Hanasaki, N., Kanae, S., Oki, T., Masuda, K., Motoya, K., Shirakawa, N., Shen, Y., and Tanaka, K.: An integrated model for the assessment of global water resources Part 2: Applications and assessments, *Hydrol. Earth Syst. Sci.*, 12, 1027–1037, 2008, <http://www.hydrol-earth-syst-sci.net/12/1027/2008/>.
- Huffman, G. J., Adler, R. F., Morrissey, M. M., Bolvin, D. T., Curtis, S., Joyce, R., McGavock, B., and Susskind, J.: Global precipitation at one-degree daily resolution from multisatellite observations, *J. Hydrometeorol.*, 2, 36–50, 2001.
- Hulme, M., Osborn, T. J., and Johns, T. C.: Precipitation sensitivity to global warming: comparison of observations with HadCM2 simulations, *Geophys. Res. Lett.*, 25(17), 3379–3382, 1998.
- Hunger, M. and Dll, P.: Value of river discharge data for global-scale hydrological modeling, *Hydrol. Earth Syst. Sci.*, 12, 841–861, 2008, <http://www.hydrol-earth-syst-sci.net/12/841/2008/>.
- ICOLD: World Register of Dams, International Commission on Large Dams (ICOLD), 1998.
- ICOLD: World Register of Dams, International Commission on Large Dams (ICOLD), 2003.
- Kendy, E. and Bredehoeft, J. D.: Transient effects of groundwater pumping and surface-water-irrigation returns on streamflow, *Water Resour. Res.*, 42, W08415, doi:10.1029/2005WR004792, 2006.
- Knighton, D.: *Fluvial forms and Processes: a new perspective*, John Wiley & Sons, Arnold, London, 383 pp., 1998.
- Labat, D., Godderis, Y., Probst, J. L., and Guyot, J. L.: Evidence for global runoff increase related to climate warming, *Adv. Water Resour.*, 27, 631–642, 2004.
- Lehner, B., Verdin, K., and Jarvis, A.: New global hydrography derived from spaceborne elevation data, *EOS Transactions*, 89, 93–94, 2008.
- Lettenmaier, D. P.: Macroscale hydrology: Challenges and opportunities, in: *Present and future of modeling global environmental change: toward integrated modeling*, edited by: Matsuno, T., and Kida, H., TERRAPUB, 111–136, 2001.
- Linderholm, H. W., Walther, A., and Chen, D. L.: Twentieth-century trends in the thermal growing season in the Greater Baltic Area, *Climatic Change*, 87, 405–419, 2008.
- Maclean, J. L., Dawe, D. C., Hardz, B., and Hettel, G. P.: *Rice almanac*, CAB Publishing, 2002.
- McCully, P.: *Silenced rivers: the ecology and politics of large dams*, Zed books, London, UK, 353 pp., 1996.
- Menzel, A., Jakobi, G., Ahas, R., Scheffinger, H., and Estrella, N.: Variations of the climatological growing season (1951–2000) in Germany compared with other countries, *Int. J. Climatol.*, 23, 793–812, 2003.
- Mialhe, F., Gunnell, Y., and Mering, C.: Synoptic assessment of water resource variability in reservoirs by remote sensing: General approach and application to the runoff harvesting systems of south India, *Water Resour. Res.*, 44, W05411, doi:10.1016/j.pce.2008.08.005, 2008.
- Micklin, P.: The Aral Sea disaster, *Annu. Rev. Earth Pl. Sc.*, 35, 47–72, 2007.
- Milliman, J. D., Farnsworth, K. L., Jones, P. D., Xu, K. H., and Smith, L. C.: Climatic and anthropogenic factors affecting river discharge to the global ocean, 1951–2000, *Global Planet. Change*, 62, 187–194, 2008.
- Milly, P. C. D., Dunne, K. A., and Vecchia, A. V.: Global pattern of trends in streamflow and water availability in a changing climate, *Nature*, 437, 347–350, 2005.
- Mitchell, T. D. and Jones, P. D.: An improved method of constructing a database of monthly climate observations and associated high-resolution grids, *Int. J. Climatol.*, 25, 693–712, 2005.
- Monfreda, C., Ramankutty, N., and Foley, J. A.: Farming the planet: 2. Geographic distribution of crop areas, yields, physiological types, and net primary production in the year 2000, *Global Biogeochem. Cy.*, 22, GB1022, GB1022, doi:10.1029/2007GB002947, 2008.
- Moore, N. and Rojstaczer, S.: Irrigation-induced rainfall and the great plains, *J. Appl. Meteorol.*, 40, 1297–1309, 2001.
- Nezlin, N. P., Kostianoy, A. G., and Lebedev, S. A.: Interannual variations of the discharge of Amu Darya and Syr Darya estimated from global atmospheric precipitation, *J. Mar. Syst.*, 47, 67–75, 2004.
- Oki, T., and Sud, Y. C.: Design of total runoff integrating pathways (TRIP)–A global river channel network, *Earth Interact.*, 2, 2–36, 1998.
- Oki, T., and Kanae, S.: Global hydrological cycles and world water resources, *Science*, 313, 1068–1072, 2006.
- Oudin, L., Hervieu, F., Michel, C., Perrin, C., Andreassian, V., Anctil, F., and Loumagne, C.: Which potential evapotranspiration input for a lumped rainfall-runoff model? Part 2 – Towards a simple and efficient potential evapotranspiration model for rainfall-runoff modelling, *J. Hydrol.*, 303, 290–306, 2005.
- Peterson, B. J., Holmes, R. M., McClelland, J. W., Vorosmarty, C. J., Lammers, R. B., Shiklomanov, A. I., Shiklomanov, I. A., and Rahmstorf, S.: Increasing river discharge to the Arctic Ocean, *Science*, 298, 2171–2173, 2002.
- Piao, S. L., Friedlingstein, P., Ciais, P., de Noblet-Ducoudre, N., Labat, D., and Zaehle, S.: Changes in climate and land use have a larger direct impact than rising CO₂ on global river runoff trends, *Proc. Natl. Acad. Sci. USA.*, 104, 15242–15247, 2007.
- Pimentel, D., Berger, B., Filiberto, D., Newton, M., Wolfe, B., Karabinakis, E., Clark, S., Poon, E., Abbett, E., and Nandagopal, S.: *Water resources: Agricultural and environmental issues*, Bioscience, 54, 909–918, 2004.
- Ponce, V. M.: *Engineering Hydrology: Principles and Practices*, Prentice Hall, 1994.
- Qian, T., Dai, A., and Trenberth, K. E.: Hydroclimatic trends in the Mississippi river basin from 1948 to 2004, *J. Climate*, 20, 4599–4613, 2007.
- Rawlins, M. A., Lammers, R. B., Frolking, S., Fekete, B. M., and Vörösmarty, C. J.: Simulating pan-Arctic runoff with a macro-scale terrestrial water balance model, *Hydrol. Process.*, 17, 2521–2539, 2003.
- Rawlins, M. A., Willmott, C. J., Shiklomanov, A., Linder, E., Frolking, S., Lammers, R. B., and Vörösmarty, C. J.: Evaluation of trends in derived snowfall and rainfall across Eurasia and linkages with discharge to the Arctic Ocean, *Geophys. Res. Lett.*, 33, L07403, doi:10.1029/2005GL025231, 2006.

- Rost, S., Gerten, D., Bondeau, A., Lucht, W., Rohwer, J., and Schaphoff, S.: Agricultural green and blue water consumption and its influence on the global water system, *Water Resour. Res.*, 44, W09405, doi:10.1029/2007WR006331, 2008.
- Rudolf, B., Beck, C., Grieser, J., and Schneider, U.: Global Precipitation Analysis Products, Deutscher Wetterdienst (DWD), 2005.
- Seitzinger, S. P., Styles, R. V., Boyer, E. W., Alexander, R. B., Billen, G., Howarth, R., Mayer, B., and van Breemen, N.: Nitrogen retention in rivers: model development and application to watersheds in the northeastern USA, *Biogeochemistry*, 57, 199–237, 2002.
- Serreze, M. C., Barrett, A. P., Slater, A. G., Woodgate, R. A., Aagaard, K., Lammers, R. B., Steele, M., Moritz, R., Meredith, M., and Lee, C. M.: The large-scale freshwater cycle of the Arctic, *J. Geophys. Res.-Oceans*, 111, C11010, doi:10.1029/2005JC003424, 2006.
- Shibuo, Y., Jarsjo, J., and Destouni, G.: Hydrological responses to climate change and irrigation in the Aral Sea drainage basin, *Geophys. Res. Lett.*, 34, L21406, doi:10.1029/2007GL031465, 2007.
- Shiklomanov, I. A. and Rodda, J. C.: World water resources at the beginning of the 21st century, UNESCO International Hydrology Press ed., Cambridge University Press, 2003.
- Siebert, S., Döll, P., Feick, S., and Hoogeveen, J.: Global map of irrigated areas version 2.2, Johann Wolfgang Goethe University, Frankfurt am Main, Germany / Food and Agriculture Organization of the United Nations, Rome, Italy, 2005a.
- Siebert, S., Döll, P., Hoogeveen, J., Faures, J.-M., Frenken, K., and Feick, S.: Development and validation of the global map of irrigation areas, *Hydrol. Earth Syst. Sci.*, 9, 535–547, 2005b, <http://www.hydrol-earth-syst-sci.net/9/535/2005/>.
- Siebert, S., and Döll, P.: Irrigation water use – a global perspective, in: *Global Change: enough water for all?*, edited by: Lozand, J. L., Menzel, H. G. L., Schönwiese, C. D., Universität Hamburg/GEO, 104–107, 2007.
- Singh, D. K. and Singh, A. K.: Groundwater situation in India: Problems and Perspective, *Int. J. Water Resour. D.*, 18, 562–580, 2002.
- Sitch, S., Smith, B., Prentice, I. C., Arneth, A., Bondeau, A., Cramer, W., Kaplan, J. O., Levis, S., Lucht, W., Sykes, M. T., Thonicke, K., and Venevsky, S.: Evaluation of ecosystem dynamics, plant geography and terrestrial carbon cycling in the LPJ dynamic global vegetation model, *Glob. Change. Biol.*, 9, 161–185, 2003.
- Snoussi, M., Hiada, S., and Imassi, S.: Effects of the construction of dams on the water and sediment fluxes of the Moulouya and the Sebou rivers, Morocco, *Reg. Environ. Change*, 3, 5–12, 2002.
- Soumis, N., Duchemin, E., Canuel, R., and Lucotte, M.: Greenhouse gas emissions from reservoir in the western United States, *Global Biogeochem. Cy.*, 18, GB3022, doi:10.1029/2003GB002197, 2004.
- Srivastava, R. C.: Design of runoff recycling irrigation system for rice cultivation, *J. Irrig. Drain. E-ASCE*, 122, 331–335, 1996.
- Srivastava, R. C.: Methodology for design of water harvesting system for high rainfall areas, *Agr. Water Manage.*, 47, 37–53, 2001.
- St. Louis, V., Kelly, C. A., Duchemin, E., Rudd, J. W. M., and Rosenberg, D. M.: Reservoir Surfaces as sources of greenhouse gases to the atmosphere: A global estimate, *BioScience*, 50, 766–775, 2000.
- Thenkabail, P. S., Biradar, C. M., Turrall, H., Noojipady, P., Li, Y. J., Vithanage, J., Dheeravath, V., Velpuri, M., Schull, M., Cai, X. L., and Dutta, R.: An Irrigated Area Map of the World (1999) derived from Remote Sensing, International Water Management Institute (IWMI), 2006.
- Tian, X., Dai, A., Yang, D., and Xie, Z.: Effects of precipitation-bias correction on surface hydrology over northern latitudes, *Geophys. Res. Lett.*, 112, D14101, doi:10.1029/2007JD008420, 2007.
- Trenberth, K. E. and Dai, A.: Effects of Mount Pinatubo volcanic eruption on the hydrological cycle as an analog of geoengineering, *Geophys. Res. Lett.*, 34, L15702, doi:10.1029/2007GL030524, 2007.
- van Werkhoven, K., Wagener, T., Reed, P., and Tang, Y.: Characterization of watershed model behavior across a hydroclimatic gradient, *Water Resour. Res.*, 44, W01429, doi:10.1029/2007WR006271, 2008.
- Vörösmarty, C. J., Willmott, C. J., Choudhury, B. J., Schloss, A. L., Stearns, T. K., Robeson, S. M., and Dorman, T. J.: Analyzing the discharge regime of a large tropical river through remote sensing, ground-based climatic data, and modeling, *Water Resour. Res.*, 32, 3137–3150, 1996.
- Vörösmarty, C. J., Sharma, K. P., Fekete, B. M., Copeland, A. H., Holden, J., Marble, J., and Lough, J. A.: The storage and aging of continental runoff in large reservoir systems of the world, *Ambio*, 26, 210–219, 1997.
- Vörösmarty, C. J., Federer, C. A., and Schloss, A. L.: Potential evaporation functions compared on US watersheds: Implications for global-scale water balance and terrestrial ecosystem modeling, *J. Hydrol.*, 207, 147–169, 1998.
- Vörösmarty, C. J., Fekete, B. M., Meybeck, M., and Lammers, R. B.: A simulated topological network representing the global system of rivers at 30-min spatial resolution (STN-30), *Global Biogeochem. Cy.*, 14, 599–621, 2000a.
- Vörösmarty, C. J., Fekete, B. M., Meybeck, M., and Lammers, R. B.: Geomorphometric attributes of the global system of rivers at 30-min spatial resolution (STN-30), *J. Hydrol.*, 237, 17–39, 2000b.
- Vörösmarty, C. J., Green, P., Salisbury, J., and Lammers, R. B.: Global water resources: Vulnerability from climate change and population growth, *Science*, 289, 284–288, 2000c.
- Vörösmarty, C. J., and Sahagian, D.: Anthropogenic disturbance of the terrestrial water cycle, *BioScience*, 50, 753–765, 2000.
- Vörösmarty, C. J.: Global water assessment and potential contributions from Earth system science, *Aquat. Sci.*, 64, 328–351, 2002.
- Vörösmarty, C. J., Meybeck, M., Fekete, B. M., Sharma, K., Green, P., and Syvitski, J.: Anthropogenic sediment retention: Major global-scale impact from the population of registered impoundments, *Global Planet. Change*, 39, 169–190, 2003.
- Vörösmarty, C. J., Leveque, C., Revenga, C., Caudill, C., Chilton, J., Douglas, E. M., Meybeck, M., and Prager, D.: Chapter 7: Fresh water ecosystems, in: *Millennium Ecosystem Assessment, 1, Conditions and Trends Working Group Report*, Island Press, 2005.
- Vörösmarty, C. J., Ericson, J. P., Dingman, S. L., Ward, L. G., and Meybeck, M.: Future impacts of fresh water resource management: sensitivity of coastal deltas, *Water Quality and Sediment Behaviour of the Future: Predictions for the 21st Century*, Perugia, Italy, 2007.

- Wheida, E. and Verhoeven, R.: Review and assessment of water resources in Libya, *Water International*, 31, 295–309, 2006.
- Willmott, C. J.: On the validation of models, *Phys. Geogr.*, 1, 184–194, 1981.
- Willmott, C. J., Rowe, C. M., and Mintz, Y.: Climatology of the Terrestrial Seasonal Water Cycle, *J. Climatol.*, 5, 589–606, 1985.
- Wisser, D., Frolking, S., Douglas, E. M., Fekete, B. M., Vörösmarty, C. J., and Schumann, A. H.: Global irrigation water demand: Variability and uncertainties arising from agricultural and climate data sets, *Geophys. Res. Lett.*, 35, L24408, doi:10.1029/2008GL035296, 2008.
- Wollheim, W. M., Vörösmarty, C. J., Bouwman, A. F., Green, P., Harrison, J., Linder, E., Peterson, B. J., Seitzinger, S. P., and Syvitski, J. P. M.: Global N removal by freshwater aquatic systems using a spatially distributed, within-basin approach, *Global Biogeochem. Cy.*, 22, GB2026, doi:10.1029/2007GB002963, 2008.